Arabidopsis ACINUS is O-glycosylated and regulates transcription and alternative splicing of regulators of reproductive transitions

Yang Bi[1], Zhiping Deng[1], Weimin Ni[1,2], Ruben Shretha[1], Dasha Savage[1], Thomas Hartwig[1], Sunita Patil[1], Su Hyun Hong[1], Juan A. Oses-Prieto[3], Kathy H. Li[3], Peter H Quail[2], Alma L Burlingame[3], Shou-Ling Xu[1*], and Zhi-Yong Wang[1*]

[1]Department of Plant Biology, Carnegie Institution for Science, Stanford, CA 94305, USA

[2]Plant Gene Expression Center, United States Department of Agriculture/Agriculture Research Service, Albany, CA94710

[3]Department of Pharmaceutical Chemistry, University of California, San Francisco, San Francisco, CA 94158, USA

[*]Authors for correspondence:

Zhiyong Wang: zywang24@stanford.edu

Shouling Xu: slxu@stanford.edu

Key words: alternative splicing, ACINUS, O-GlcNAc, seed dormancy, flowering

Abstract

O-GlcNAc modification plays important roles in metabolic regulation of cellular status. Two homologs of O-GlcNAc transferase, SECRET AGENT (SEC) and SPINDLY (SPY), which have O-GlcNAc and O-fucosyl transferase activities, respectively, are essential in *Arabidopsis* but have largely unknown cellular targets. Here we show that AtACINUS is O-GlcNAcylated and O-fucosylated and mediates regulation of transcription, alternative splicing (AS), and developmental transitions. Knocking-out both AtACINUS and its distant paralog AtPININ causes severe growth defects including dwarfism, delayed seed germination and flowering, and abscisic acid (ABA) hypersensitivity. Transcriptomic and protein-DNA/RNA interaction analyses demonstrate that AtACINUS represses transcription of the flowering repressor *FLC* and mediates AS of *ABH1* and *HAB1*, two negative regulators of ABA signaling. Proteomic analyses show AtACINUS's O-GlcNAcylation, O-fucosylation, and association with splicing factors, chromatin remodelers, and transcriptional regulators. Some AtACINUS/AtPININ-dependent AS events are altered in the *sec* and *spy* mutants, demonstrating a function of O-glycosylation in regulating alternative RNA splicing.

Introduction

Posttranslational modification of intracellular proteins by O-linked *N*-acetylglucosamine (O-GlcNAc) is an important regulatory post-translational modification (PTM) that modulates protein activities and thereby control cellular functions according to nutrient and energy status[1,2]. Extensive studies in animals have shown that thousands of proteins involved in diverse biological processes are modified on serine and threonine residues by O-GlcNAcylation, which is catalyzed by O-GlcNAc transferase (OGT) using UDP-GlcNAc as donor substrate[1,3]. As a sensor of primary metabolic status, O-GlcNAcylation plays key roles in cellular homeostasis and responses to nutritional and stress factors[1,2,4,5], whereas dysregulation of O-GlcNAcylation has been implicated in many diseases including cancer, diabetes, cardiovascular and neurodegenerative diseases[5,6]. The *Arabidopsis* genome encodes two OGT homologs: SPINDLY (SPY) and SECRET AGENT (SEC). The *spy* mutant was identified as a gibberellin (GA) response mutant with phenotypes of enhanced seed germination, early flowering, increased stem elongation, and hyposensitivity to the stress hormone abscisic acid (ABA)[7,8]. The *sec* mutants show no dramatic phenotype, but the double loss-of-function *spy sec* mutants are embryo lethal[9]. SEC and SPY were recently reported to have O-GlcNAc and O-fucosyl transferase activities, respectively, and they antagonistically regulate DELLAs, the repressors of GA signaling[10]. The lethal phenotype of *spy sec* double mutants suggests that SPY and SEC have broader functions, which remain to be investigated at the molecular level[10-12]. Our recent study identified the first large set of 971 O-GlcNAcylated peptides in 262 *Arabidopsis* proteins[13]. The functions of these O-GlcNAcylation events remain to be characterized.

One of the O-GlcNAcylated proteins is AtACINUS, an *Arabidopsis* homolog of the mammalian apoptotic chromatin condensation inducer in the nucleus (Acinus)[14]. In animals, Acinus forms the apoptosis and splicing-associated protein (ASAP) complex by recruiting RNA-binding protein S1 (RNPS1), a peripheral splicing factor, and Sin3-associated protein of 18 kDa (SAP18), a chromatin remodeler, through its conserved RNPS1-SAP18 binding (RSB) domain[14]. Another RSB-containing protein, Pinin, forms a similar protein complex named PSAP, which has distinct biological functions[14,15]. The

ASAP and PSAP complexes are believed to function at the interface between histone modification, transcription, and alternative splicing (AS) in metazoans[14,16,17]. In *Arabidopsis*, AtRNPS1, also known as ARGININE/SERINE-RICH 45 (SR45), has been implicated in splicing, transcription and RNA-dependent DNA methylation, with effects on multiple aspects of plant development as well as stress and immune responses[18-23]. AtSAP18 has been shown to associate with transcription factors involved in stress responses and embryo development[24,25]. AtACINUS, AtSAP18 and SR45 have been shown to associate with a transcription factor involved in flowering[26]. While sequence analysis predicted similar ASAP complex in plants[23], interactions among SR45, AtSAP18, and AtACINUS remain to be tested experimentally and the functions of AtACINUS and AtPININ remain to be characterized genetically.

Our finding of O-GlcNAcylation of AtACINUS suggests that the functions of AtACINUS are regulated by O-linked glycosylation[13]. We therefore performed genetic, genomic, and proteomic experiments to understand the functions of AtACINUS and its regulation by O-linked sugar modifications. Our results demonstrate key functions of AtACINUS and its distance homology AtPININ in regulating seed germination, ABA sensitivity, and flowering, through direct involvement in AS of two key components of the abscisic acid (ABA) signaling pathway and in the transcriptional regulation of the floral repressor *FLC*. Our results further show that AtACINUS is modified by both O-GlcNAc and O-fucose, is part of the ASAP complex, and associates with splicing and transcription factors. A subset of AtACINUS-dependent AS events is altered in the *spy* and *sec* mutants, providing genetic evidence for regulation of AS by the O-linked glycosylations.

Result

AtACINUS and *AtPININ* play genetically redundant roles

The *Arabidopsis* AtACINUS (AT4G39680) protein is 633 amino-acid long, and it shares sequence similarity to all the known motifs of the human Acinus including the N-terminal SAF-A/B, Acinus and PIAS (SAP) motif, the RNA-recognition motif (RRM) and the C-terminal RSB motif (Fig. 1a, Supplementary Fig. 1a)[14,16,27]. AtACINUS is a unique

gene in *Arabidopsis* with no homolog detectable using standard BLAST (Basic Local Alignment Search Tool) search of the *Arabidopsis* protein database. However, another *Arabidopsis* gene (AT1G15200, AtPININ) contains the RSB domain and is considered a homolog of mammalian Pinin[14]. AtACINUS and AtPININ share 12 amino acids within the 15-amino acid region of RSB motif (Fig. 1b), but no sequence similarity outside this motif.

To study the biological function of AtACINUS, we obtained two mutant lines that contain T-DNA insertions in the exons of *AtACINUS*, *Salk_078854* and *WiscDsLoxHs108_01G*, which are designated *acinus-1* and *acinus-2,* respectively (Fig. 1c). These mutants showed no obvious morphological phenotypes except slightly delayed flowering (Fig. 1d,e). The weak phenotype of *acinus* is surprising considering the important function of its mammalian counterpart and the absence of any close homolog in *Arabidopsis*.

We did not expect AtACINUS and AtPININ to have redundant functions, considering their very limited sequence similarity and the fact that mammalian Acinus and Pinin have distinct functions[14]. AtPININ shares extensive sequence similarity with human Pinin surrounding the RSB domain[14] (Supplementary Fig. 1b). Phylogenetic analysis indicated that AtPININ and human Pinin belong to one phylogenetic branch that is distinct from that of AtACINUS and human Acinus (Supplementary Fig. 1c), suggesting independent evolution of ACINUS and PININ before the separation of the metazoan and plant kingdoms. However, Pinin can, through its RSB domain, interact with RNPS1 and SAP18 to form a complex (PSAP) similar to the ASAP complex. Therefore, we tested the possibility that the weak phenotype of *Arabidopsis acinus* mutants is due to functional redundancy with AtPININ.

We obtained a T-DNA insertion mutant of AtPININ (*pinin-1*, T-DNA line *GABI_029C11*). The *pinin-1* mutant also showed no obvious morphological phenotype (Fig. 1d). We then crossed *pinin-1* with *acinus-1* and *acinus-2* to obtain double mutants. Both *acinus-1 pinin-1* and *acinus-2 pinin-1* double mutants displayed pleiotropic phenotypes including severe dwarfism, short root, pale leaves, narrow and twisted rosette leaves with serrated margin, severely delayed flowering, altered phyllotaxis,

increased numbers of cotyledons and petals, and reduced fertility (Fig. 1d,e, and Supplementary Fig. 2). The *acinus-2 pinin-1* double mutants transformed with *35S::AtACINUS-GFP* or *35S::YFP-AtPININ* displayed near wild-type morphology (Fig. 1f), confirming that the phenotypes of the double mutants are due to loss of both AtACINUS and AtPININ, and the two genes play genetically redundant roles. The AtACINUS-GFP and YFP-AtPININ proteins are localized in the nucleus outside the nucleolus (Supplementary Fig. 3).

We also noticed that the seed germination was delayed in the *acinus pinin* mutant (Fig. 2a). This, together with the pale leaf and dwarfism phenotypes, suggests an alteration in ABA response. Indeed, on 0.25 µmol/L ABA, germination of the *acinus-2 pinin-1* double mutant seeds was further delayed compared to the wild type and the single mutants (Fig. 2b). Dose response experiment indicate that seed germination of the *acinus-1 pinin-1* and *acinus-2 pinin-1* double mutants is about three fold more sensitive to ABA than wild type and the *acinus* and *pinin* single mutants (Fig. 2c). Similarly, post-germination seedling growth of *acinus-2 pinin-1* was more inhibited by ABA (Supplementary Fig. 4a). These ABA-hypersensitive phenotypes were rescued by expression of either AtACINUS-GFP or YFP-AtPININ in the *acinus-2 pinin-1* background (Fig. 2d and Supplementary Fig. 4b). These results indicate that the *acinus-2 pinin-1* double mutant is hypersensitive to ABA, and that AtACINUS and AtPININ are redundant negative regulators of ABA responses.

AtACINUS and AtPININ are involved in AS of specific introns

We conducted RNA-seq analysis of the transcriptome of the *acinus-2 pinin-1* double mutant. Wild-type and *acinus-2 pinin-1* seedlings were grown under constant light for 14 days, and RNA-seq was performed with three biological replicates, each yielding a minimum of 22.4 million uniquely mapped reads. The RNA-seq data confirmed the truncation of the *AtACINUS* and *AtPININ* transcripts in the double mutant (Supplementary Fig. 5). Compared to wild type, the *acinus-2 pinin-1* double mutant showed significantly decreased expression levels for 786 genes and increased levels of 767 genes (fold change>2, multiple-testing corrected p-value<0.05), which include the flowering repressor *FLC*[28] (Supplementary Data 1).

A significantly higher proportion of reads was mapped to the intron regions in the *acinus-2 pinin-1* double mutant than in the wild type (Supplementary Fig. 6a). Further analyses using the RACKJ software package revealed increase of retention of 258 introns in 225 genes and decreased retention of 31 introns in 31 genes in the *acinus-2 pinin-1* double mutant compared to wild type (Fig. 3a, Supplementary Data 2). Intron retention was the dominant form of splicing defect in the *acinus-2 pinin-1* double mutant (Fig. 3a, Supplementary Fig. 6b). About 99% of these genes contain multiple introns, and the defects tend to be retention of a specific single intron among many introns of each gene, indicating defects in alternative splicing rather than general splicing. Among the RNAs showing increased intron retention, 26 RNAs also showed decreased levels of RNA abundance, and their retained introns introduce in-frame stop codons (Supplementary Fig. 7), consistent with non-sense-mediated decay[29]. The results show that AtACINUS and AtPININ function in AS, primarily by enhancing splicing of a specific intron among many introns of each transcript.

We found a significant overlap between ABA-induced genes and the genes overexpressed in *acinus-2 pinin-1* (p-value by random chance <2.42E-13) (Fig. 3b). Only four of these RNAs were mis-spliced in *acinus-2 pinin-1*. One possibility is that intron retention in RNAs encoding components of ABA synthesis or signaling pathway leads to expression of ABA-responsive genes. Indeed, we found retention of the 10th intron of *ABA HYPERSENSIVE 1* (*ABH1)* in the *acinus-2 pinin-1* double mutant (Fig. 4a).

ABH1 encodes the large subunit of the dimeric *Arabidopsis* mRNA cap-binding complex (NUCLEAR CAP-BINDING PROTEIN SUBUNIT 1, CBP80) and functions as a negative regulator of ABA responses including inhibition of seed germination[30,31]. The retention of the 10th intron of ABH1 introduces a pre-mature stop codon that truncates the C-terminal 522 amino acids of ABH1 (Fig. 4a). Quantification using qRT-PCR analysis in 12-day-old seedlings showed that the intron-containing *ABH1.2* transcript was about 8-10% of the total *ABH1* transcripts in the wild type, about 11% in *pinin-1*, about 15% in *acinus-2*, but more than 50% in *acinus-2 pinin-1* (Fig. 4b,c). Expression of either YFP-AtPININ or AtACINUS-GFP in the *acinus-2 pinin-1* background rescued the

ABH1 intron retention phenotype (Fig. 4b,c). Consistent with compromised *ABH1* activity, the gene expression changes in *acinus-2 pinin-1* show a strong correlation to those in *abh1*, with Spearman's correlation=0.74 as calculated by AtCAST3.1 (Supplementary Fig. 8)[32,33].

Intron retention in *HAB1* has been reported to cause ABA hypersensitive phenotypes[34,35]. *HAB1* did not display any apparent splicing defects in our RNA-seq and RT-PCR analysis of 12-day old seedling. However, after ABA treatment, *HAB1* intron retention is significantly increased in *acinus pinin* compared to the wild type. While the expression level of *HAB1* transcripts was increased similarly in wild type and *acinus pinin,* the wild-type seedlings maintained relatively similar ratios between different splice forms of *HAB1* before and after ABA treatment, whereas the *acinus pinin* mutant accumulated a much increased level of the intron-containing *HAB1.2* and a reduced level of fully spliced *HAB1.3* after ABA treatment (Fig. 4d,e). *HAB1.2* encodes a dominant negative form of HAB1 protein that activates ABA signaling[34,35]. Therefore, the accumulation of HAB1.2 should contribute to the ABA hypersensitivity of the *acinus pinin* mutant.

To test whether AtACINUS is directly involved in AS of *ABH1* and *HAB1*, we carried out an RNA immunoprecipitation (RIP) experiment using an *AtACINUS-GFP/acinus-2* transgenic line, with *35S::GFP* transgenic plants as the negative control. Immunoprecipitation using an anti-GFP antibody pulled down significantly more *ABH1* and *HAB1* RNAs in *AtACINUS-GFP/acinus-2* than in the *35S::GFP* control (Fig. 4f,g), indicating that AtACINUS interacts with *ABH1* and *HAB1* RNAs *in vivo* and is involved in their splicing.

AtACINUS regulates flowering through repression of *FLC*

Consistent with the late flowering phenotype of *acinus pinin* (Fig. 1e, 5a), our RNA-seq data showed an increased expression level of the floral repressor *FLC*, without obvious alteration of the splicing pattern (Supplementary Fig. 9a). RT-qPCR analysis confirmed the increased levels of *FLC* RNA that correspond to the severity of the late-flowering phenotypes in the single and double mutants (Fig. 5b). As *FLC* expression is also controlled by its anti-sense RNA, which undergoes AS[36,37], we

analyzed the anti-sense *FLC* RNAs using RT-qPCR. The results showed a dramatic increase of the class I anti-sense RNA and a slight increase of the class II anti-sense RNA of *FLC*, but no obvious change of the splicing efficiency of the *FLC* anti-sense RNAs (Supplementary Fig. 9b-d). AtACINUS was recently reported to associate with VAL1 and VAL2, which bind to the *FLC* promoter to repress transcription[26]. We thus performed chromatin immunoprecipitation (ChIP) assays to test whether AtACINUS is associated with the *FLC* locus, and our results show that AtACINUS interacts with the DNA of the promoter and first intron regions but not the 3' region of *FLC in vivo* (Fig. 5c). Together our results provide evidence for a role of AtACINUS in regulating the transcription of *FLC*.

AtACINUS-dependent AS events are altered in *spy* and *sec*

To study how O-linked sugar modification affects the function of AtACINUS, we tested if the AtACINUS-dependent AS events are altered in the *spy* and *sec* mutants. Of the ten AtACINUS-dependent intron splicing events we have tested, four showed alterations in the *spy* mutant and one showed alteration in the *sec* mutant (Fig. 6).

In the 7-day-old light-grown plants, splicing of the 12th intron and the 15th intron of *TRNA METHYLTRANSFERASE 4D* (*TRM4D*, *At4g26600*) was enhanced in the *acinus-2 pinin* double mutant compared to that in the WT. In the loss-of-function mutants *spy-4* and *spy-t1* (SALK_090580), the splicing efficiency of these two introns were also enhanced. In contrast, the loss-of-function mutants *sec-2* and *sec-5* showed an increased retention of the 12th intron (Fig. 6). These results suggest that SPY and SEC have opposite effects on AtACINUS function in *TRM4D* splicing. The *spy-t1* and *spy-4* mutants accumulated more *HAB1.3* and less *HAB1*.2 than wild type, while *acinus-2 pinin* accumulated more *HAB1.2* than the wild type (Fig. 6), consistent with their opposite seed germination phenotypes. In addition, the splicing efficiency of the 14th intron of *EMBRYO DEFECTIVE 2247* (*Emb2247*, *AT5G16715*) was reduced in the *acinus-2 pinin* double mutant, but was increased in the *spy-t1* and *spy-4* mutants compared to wild type (Fig. 6). These results support that the O-linked sugar modifications of AtACINUS modulate its functions in alternative splicing of specific RNAs.

AtACINUS associates with transcriptional and splicing factors

To understand the molecular mechanisms of AtACINUS function, we conducted two immunoprecipitations followed by mass spectrometry (IP-MS) experiments. In the first experiment, immunoprecipitation was performed in three biological replicates using the AtACINUS-GFP/*acinus-2* plants and the anti-GFP nanobody. Transgenic plants expressing a Tandem-Affinity-Purification-GFP (TAP-GFP) protein was used as control[38]. The proteins co-immunoprecipitated with AtACINUS-GFP was identified based on enrichment (FDR=0.01, S0=2) relative to the TAP-GFP control, quantified by label-free mass spectrometry analysis. In the second experiment, AtACINUS-associated proteins were identified by ^{15}N stable-isotope-labeling in *Arabidopsis* (SILIA) quantitative MS. Wild-type and *acinus-2* mutant seedlings were metabolically labelled with ^{14}N and ^{15}N, and immunoprecipitation was performed using the anti-AtACINUS antibody, followed by mass spectrometry analysis. The isotope labels were switched in the two biological replicates. AtACINUS-associated proteins were identified based on enrichment in the wild type compared to the *acinus* mutant control. These IP-MS experiments consistently identified 46 AtACINUS-associated proteins (Fig. 7a, Supplementary Fig. 10a and Supplementary Data 3). These included SR45 and AtSAP18, supporting the existence of an evolutionarily conserved ASAP complex in *Arabidopsis*. The AtACINUS interactome also included a large number of proteins homologous to known components of the spliceosome, including five Sm proteins, one protein of the U2 complex, four proteins in the U5 complex, seventeen proteins of the nineteen complex (NTC) and NTC-related complex (NTR)[39-41]. In addition, AtACINUS associated with six proteins of the exon junction complex (EJC) core and the EJC-associated TRanscription-EXport (TREX) complex, three proteins of the small nucleolar ribonucleoprotein (snoRNP) complexes, and four other splicing-related proteins (Fig. 7a, Supplementary Data 3)[41-45]. AtACINUS interactome also included a component of the RNA Polymerase II Associated Factor 1 Complex (PAF1C) (Fig. 7a, Supplementary Data 3). The interactome data suggests that, similar to mammalian Acinus, AtACINUS plays dual roles in AS and transcriptional regulation.

The AtACINUS interactome includes five proteins that are genetically involved in regulating *FLC* and flowering (Fig. 7a, Supplementary Data 3). These are BRR2 and PRP8 of the U5 complex, ELF8 of the PAF1C, and SR45 and AtSAP18 of the ASAP complex[19,37,46,47]. These results suggest that AtACINUS may regulate *FLC* expression through a complex protein network involving multiple regulatory pathways.

We have previously identified O-GlcNAcylation modification on Thr79 on AtACINUS[13] (Fig. 7b) after LWAC enrichment. Mass spectrometry analysis following affinity purification of AtACINUS identified additional O-GlcNAc modification on the peptide containing amino acids 407-423 (Fig. 7c, Supplementary Fig. 10b), as well as O-fucosylation on the peptide containing amino acids 169-197 (Fig. 7d). These results confirm that AtACINUS is a target of both O-GlcNAc and O-fucose modifications.

Using targeted mass spectrometry analysis, we confirmed that the *acinus-2 pinin* double mutant expressed only the AtACINUS's N-terminal peptides (at about 20% wild-type level), but no detectable peptides of the C-terminal region (after T-DNA insertion) (Supplementary Fig 11, Supplementary Table 5). Both N- and C-terminal peptides of AtPININ were undetectable in the *acinus-2 pinin* mutant (Supplementary Fig 12, Supplementary Table 5). Meanwhile, SR45 and AtSAP18 protein levels were dramatically reduced to 3.9% and 2.7% of wild-type levels, respectively (Supplementary Fig. 13 and 14, Supplementary Table 5). Together, these results indicate that the stability of the other members of the ASAP and PSAP complexes is dependent on AtACINUS and AtPININ.

Discussion

Our recent identification of O-GlcNAcylated proteins in *Arabidopsis* enabled functional study of this important signaling mechanism in plants[13]. Here our systematic analysis of one of these O-GlcNAcylated proteins, AtACINUS, demonstrates its functions as a target of O-GlcNAc and O-fucose signaling and a component of the evolutionarily conserved ASAP complex that regulates transcription and RNA alternative splicing thereby modulating stress responses and developmental transitions. Our comprehensive genetic, transcriptomic, and proteomic analyses provide a large body of strong evidence illustrating a molecular pathway in which nutrient sensing O-

GlcNAcylation and O-fucosylation modulate specific functions of the evolutionarily conserved RSB-domain protein AtACINUS to modulate stress hormone sensitivity, seed germination, and flowering in plants (Fig. 7e).

Studies in animals have identified Acinus and Pinin as essential cellular components that bridge chromatin remodeling, transcription and splicing through the formation of analogous ASAP and PSAP complexes[14,16,17,48-51]. Sequence alignment and phylogenetic analysis show that the *Arabidopsis* orthologs, AtACINUS and AtPININ, share higher levels of sequence similarity to their animal counterparts than to each other and appear to have evolved independently since the separation of the plant and metazoan kingdoms[14]. Considering their evolutionary distance and limited sequence similarity (12 amino acid residues in the RSB motif), it was surprising that the functions of AtACINUS and AtPININ are genetically redundant. This represents likely the least sequence similarity between two redundant genes and raises cautions for prediction of genetic redundancy based on the level of sequence similarity.

The developmental functions in seed germination and flowering seem to involve AtACINUS's distinct activities in splicing and transcription of key components of the regulatory pathways. Specifically, AS events in *ABH1* and *HAB1* are likely the major mechanisms by which AtACINUS modulates ABA signaling dynamics to control seed germination and stress responses. ABH1 is an mRNA cap-binding protein that modulates early ABA signaling[30,31]. The loss-of-function *abh1* mutant with a T-DNA insertion in the 8th intron is ABA hypersensitive with enhanced early ABA signaling[30]. Similarly, the retention of the 10th intron of *ABH1* in *acinus pinin* mutant is expected to truncate its C-terminal half and cause loss of *ABH1* function and thus increase of ABA sensitivity. Supporting the functional role of the ASAP/PSAP-ABH1 pathway, we observed a significant correlation between the transcriptomic changes in *abh1* and the *acinus pinin* double mutant (Supplementary Fig. 8)[32,33]. A recent proteomic study showed that the ABH1 protein level was decreased in the *sr45* mutant[23], whereas a reduction of *ABH1* RNA level to ~30% caused obvious phenotypes in potato[52].

AtACINUS-mediated AS of *HAB1* switches a positive feedback loop to a negative feedback loop in the ABA signaling pathway. *HAB1* encodes a phosphatase that

dephosphorylates the SNF1-related protein kinases (SnRK2s) to inhibit ABA responses, and the ligand-bound ABA receptor inhibits HAB1 to activate ABA responses[53,54]. The intron-containing *HAB1.2* encodes a dominant negative form of HAB1 protein that lacks the phosphatase activity but still competitively interacts with SnRK2, thus activating, instead of inhibiting, ABA signaling[34,35]. As ABA signaling feedback increases the *HAB1* transcript level, the AtACINUS-mediated AS switches a positive feedback loop that reinforces ABA signaling to a negative feedback loop that dampens ABA signaling. Such a switch is presumably important the different ABA signaling dynamics required for the onset of and recovery from stress responses or dormancy.

The relative contributions of intron retention of *ABH1* and *HAB1* to ABA sensitivity will need to be quantified by genetic manipulation of each splicing event. Additional mechanisms may contribute to the ABA-hypersensitivity phenotypes of *acinus pinin*. For example, the level of SR45 is significantly decreased in *acinus pinin*, while loss of SR45 has been reported to cause accumulation of SnRK1 which is a positive regulator of stress and ABA responses[55].

The late-flowering phenotype of the *acinus pinin* mutant correlated with increased *FLC* expression. A role of AtACINUS in repressing *FLC* has been suggested based on its association with the VAL1 transcription factor, which binds to the *FLC* promoter[26]. Our results provide genetic evidence for the function of AtACINUS in repressing *FLC* expression. Further, our ChIP-PCR analysis shows that AtACINUS associates with genomic DNA of the promoter region and the first intron of *FLC,* confirming a direct role in transcriptional regulation of *FLC*. These results provide critical evidence for the hypothesis that the AtACINUS represses *FLC* by AtSAP18-mediated recruitment of the Sin3 histone deacetylase complex (HDAC)[26]. It's worth noting that overexpression of AtSAP18 in the *sr45* mutant increased *FLC* expression and further delayed flowering[23]. It's possible that the transcriptional repression function of AtSAP18 requires the ASAP/PSAP complex. It's also worth noting that the AtACINUS interactome includes several proteins known to be involved in regulating *FLC* expression and flowering. Among these, BRR2 and PRP8 are components of the U5 complex and mediate splicing of the sense and anti-sense transcripts of *FLC* to inhibit and promote flowering,

respectively[37,46]. ELF8 is a component of the PAF1 complex and promotes histone methylation of *FLC* chromatin[47]. The identification of additional *FLC*-regulators as AtACINUS-associated proteins suggests that AtACINUS may regulate *FLC* expression through complex protein networks. Genetic evidence supports that ELF8/PAF1C and SR45 also have dual functions in regulating *FLC* expression and ABA responses[18,19,22,56], suggesting that the functions of AtACINUS in seed germination and flowering may involve overlapping protein networks.

Structural studies in metazoan systems showed that the RSB domains of Acinus and Pinin directly interact with RNPS1 and SAP18, forming a ternary ASAP and PSAP complexes that have both RNA- and protein-binding properties as well as abilities to interact with both RNA splicing machinery and histone modifiers[14]. ASAP and PSAP function as EJC peripheral protein complexes to modulate RNA processing[15,57]. Our quantitative proteomic analysis of the AtACINUS interactome indicates strong interaction with SR45 (ortholog of RNPS1) and AtSAP18, as well as components of EJC. Further, levels of SR45 and AtSAP18 proteins are greatly reduced in *acinus pinin*. In contrast, the *sr45* mutation leads to a similar near absence of AtSAP18 but only a mild decrease of the AtACINUS protein level[23]. Together these observations support the notion that AtACINUS and AtPININ mediate formation of similar ASAP and PSAP complexes and stabilize SR45 and AtSAP18 in plants.

Studies in human cells have shown that Acinus and Pinin mediate splicing of distinct RNAs and that Acinus cannot rescue the splicing defects caused by knockdown of Pinin[15]. In contrast, AtACINUS and AtPININ appear to have largely redundant and interchangeable functions. It's possible that both AtACINUS and AtPININ, through their RSB domain, recruit SR45 and AtSAP18, which determine target specificities. However, AtACINUS and AtPININ may have subtle differences in their functions. Like human Acinus, AtACINUS contains two additional conserved domains that are absent in AtPININ. Further, the regions of AtACINUS and AtPININ, as well as human Acinus and Pinin, outside the RSB domain contain mostly divergent intrinsically disordered sequences[58] (Supplementary Fig. 15). These distinct sequences may provide specificity in interactions with target transcripts and partner proteins or in regulation by PTMs[58].

Indeed, O-GlcNAcylated residues (Thr79 and amino acids 407-423) and the O-fucosylated site (amino acids 169-197) were in the intrinsically disordered regions of AtACINUS, whereas no O-GlcNAc or O-fucose modification was detected in AtPININ, though this could be due to partial sequence coverage of our mass spectrometry analysis. Deep RNA-seq analysis with higher sequence coverage of the single and double mutants of *acinus* and *pinin* will be required to fully understand their functional overlap and specificities.

How SEC/O-GlcNAc and SPY/O-fucose modulate development and physiology of plants is not fully understood at the molecular level. The mechanism of regulating GA signaling involves antagonistic effects of O-fucosylation and O-GlcNAcylation of the DELLA proteins[10]. Similarly, we observed opposite effect of *spy* and *sec* on the splicing of the 12th intron of *TRM4D,* suggesting distinct effects of O-GlcNAcylation and O-fucosylation on AtACINUS functions. Consistent with their different phenotype severities, more AS events were affected in *spy* than *sec*. The *spy* mutant showed increased splicing for four of the ten introns analyzed; two of these introns (in *TRM4D*) were more spliced and the other two (*HAB1* and *EMB2247)* were less spliced in the *acinus pinin* mutant than in wild type, suggesting that the SPY-mediated O-fucosylation may have different effects on AtACINUS activities on different transcripts. The two O-GlcNAc-modified residues (Thr79 and amino acids 407-423) and the O-fucose modified residue (amino acids 169-197) are in different regions of the intrinsically disordered sequence[58] (Supplementary Fig. 15), suggesting that PTMs in the disordered sequences play roles in substrate-specific splicing activities.

The high percentage of AtACINUS-dependent AS events affected in *spy* and *sec* supports an important function of AtACINUS in mediating the regulation of AS by O-glycosylation. On the other hand, AtACINUS-independent mechanisms may also contribute to the regulation, as the O-GlcNAcylated *Arabidopsis* proteins include additional RNA-binding and splicing factors[13], such as SUS2 which is in the AtACINUS interactome. Deep transcriptomic analysis of *spy*, *sec*, and conditional double *spy sec* mutants will be required to better understand how O-GlcNAc and O-fucose modulate RNA processing and AtACINUS function. Genetic analyses have suggested that SPY

435 acts upstream of the ABA insensitive 5 (ABI5) transcription factor in regulating seed
436 germination[8]. The molecular link between SPY/O-fucose and ABA signaling has
437 remained unknown. Our results support a hypothesis that O-fucose modification
438 modulates AtACINUS activity in splicing a subset of transcripts including *HAB1* to
439 modulate ABA sensitivity. The biological function of this SPY-AtACINUS pathway
440 remains to be further evaluated by genetic analyses including mutagenesis of the O-
441 fucosylation sites of AtACINUS. It is likely that parallel pathways also contribute to the
442 regulation of ABA sensitivity and seed germination by O-fucosylation and O-
443 GlcNAcylation. For example, increased GA signaling was thought to contributes to ABA
444 hyposensitivity in the *spy* mutant[59]. Further, the ABA response element binding factor 3
445 (ABF3) is also modified by O-GlcNAc[13]. The function of O-glycosylation in stress
446 responses seems to be conserved, as large numbers of molecular connections between
447 O-GlcNAc and stress response pathways have been reported in metazoans[5].

448 How O-linked glycosylation of AtACINUS affect its transcriptional activity at the
449 *FLC* locus remains to be investigated. Both *spy* and *sec* mutants flower early, opposite
450 to *acinus pinin*. While *spy* shows strong early flowering phenotype, the *FLC* expression
451 level was unaffected in *spy* under our experimental conditions (Supplementary Fig. 16),
452 suggesting that SPY regulates flowering independent of *FLC*. The *FLC* level was
453 decreased in *sec*[60], supporting the possibility that O-GlcNAcylation affects AtACINUS
454 transcription activity. However, the effect of *sec* on *FLC* expression could also be
455 mediated by other O-GlcNAc-modified flowering regulators[13,60].

456 Our study reveals important functions of AtACINUS in developmental transitions
457 and a previously unknown function of O-linked glycosylation in regulating RNA
458 alternative splicing. While we were getting our revised manuscript ready for submission,
459 evidence was reported for similar function of O-GlcNAc in intron splicing in metazoan
460 and for broad presence of stress-dependent intron retention in plants. Interestingly,
461 inhibition of OGT was found to increase splicing of detained introns in human cells[61].
462 Detained introns are a novel class of post-transcriptionally spliced (pts) introns, which
463 are one or few introns retained in transcripts where other introns are fully spliced[62].
464 Transcripts containing pts introns are retained on chromatin and are considered a

reservoir of nuclear RNA poised to be spliced and released when rapid increase of protein level is needed, such as in neuronal activities[62,63]. A recent study uncovered a large number of pts introns in *Arabidopsis*. A significant portion of these pts introns show enhanced intron retention under stress conditions. Several splicing factors involved in pts intron splicing, MAC3A, MAC3B and SKIP[64], are parts of the AtACINUS interactome. Among the introns retained in the *acinus pinin* mutant, 114 are pts introns, which is about 1.7-fold the random probability (*p* value< 3.0e-9). These pts introns include the intron retained in *ABH1* but not that in *HAB1*, consistent with translation of the dominant negative form of HAB1.2[34,35]. Together with these recent developments, our study raises the possibility that AtACINUS plays important roles in the splicing of pts introns, acting downstream of the metabolic signals transduced by SPY/O-fucose and SEC/O-GlcNAc. Our study supports an evolutionarily conserved function of O-glycosylation in regulating RNA splicing, thereby linking metabolic signaling with switches of cellular status between normal and stress conditions as well as during developmental transitions.

Material and Methods

Plant materials

All the *Arabidopsis thaliana* plants used in this study were in the Col-0 ecotype background. The plants were grown in greenhouses with a 16-h light/8-h dark cycle at 22-24^{o}C for general growth and seed harvesting. For seedlings grown on the medium in Petri dishes, the sterilized seeds were grown on ½ Murashige and Skoog (MS) medium and supplemented with 0.7% (w/v) phytoagar. Plates were placed in a growth chamber under the constant light condition at 21-22 ^{o}C. T-DNA insertional mutants for AtACINUS(AT4G39680), *atacinus-1* (Salk_078854, insertion position +674 relative to the genomic translational start site), *atacinus-2* (WiscDsLoxHs108_01G, insertion position +1744), and for AtPININ (AT1G15200) *atpinin-1* (GABI_029C11, insertion position +1817), *spy-t1* (Salk_ 090580), and *sec-5* (Salk_034290) were obtained from *Arabidopsis* Biological Resource Center. The *spy-4* and *sec-2* seeds that have been backcrossed to Columbia for six generations were provided by Neil Olszewski lab.

Germination assay

Seeds were surface sterilized with 70% (v/v) ethanol and 0.1% (v/v) Triton X-100 sterilization solution for 5 mins. The sterilization solution was then removed and seeds were re-

496 suspended in 100% ethanol and dried on a filter paper. The sterilized seeds were then plated on
497 ½ MS medium supplemented with mock or ABA. The seeds were placed in 4°C cold room for 3
498 days for stratification before moving into a growth chamber to germinate. Germination was
499 defined as obvious radicle emergence from the seed coat.

500 **Gene cloning and plant transformation**

501 The *AtACINUS* cDNA was initially cloned into the vector pENTR-D/TOPO and
502 subsequently into the binary vector pGWB5 to generate the *35S::AtACINUS-GFP* plasmid. The
503 *35S::AtACINUS-GFP* binary plasmid was transformed into *acinus-2* plants by floral dipping with
504 A. tumefaciens strain GV3101. A homozygous *35S::AtACINUS-GFP*/*acinus-2* plant was
505 selected for similar protein expression level to the endogenous AtACINUS protein of wild-type
506 plants using a native α-AtACINUS antibody, and crossed with *acinus-2 pinin-1* to obtain
507 *35S::AtACINUS-GFP*/*acinus-2 pinin-1* transgenic lines. Similarly, *35S::AtACINUS-YFP-TurboID*
508 plasmid was generated by LR reaction of gateway-compatible *35S::YFP-TbID*[65] with *pENTR-*
509 *AtACINUS* and transformed to *acinus-2 pinin-1* to obtain transgenic lines.

510 The *AtPININ* cDNA was acquired from *Arabidopsis* stock center and subsequently
511 cloned into the binary vector pEarleyGate104 to generate the *35S::YFP-AtPININ* vector. The
512 *35S::YFP-AtPININ* binary plasmid was transformed into *acinus-2 pinin-1*/+ plants by floral
513 dipping with A. tumefaciens strain GV3101. Transgenic plants were genotyped for *pinin-1* allele
514 to obtain *35S::YFP-AtPININ*/*acinus-2 pinin-1* transgenic lines.

515 **Bioinformatics analysis**

516 Dendrogram of AtACINUS and AtPININ homologs in different species was constructed
517 using the "simple phylogeny" web tool of EMBL-EBI website with UPMGA method using default
518 settings (https://www.ebi.ac.uk/Tools/phylogeny/simple_phylogeny/). The protein alignment was
519 generated using MUSCLE from EMBL-EBI website with default setting
520 (https://www.ebi.ac.uk/Tools/msa/muscle/)[66,67]. Pairwise protein sequence alignment was
521 performed with Blastp from the NCBI blastp suite with E-value set to 0.01.
522 (https://blast.ncbi.nlm.nih.gov/Blast.cgi?PAGE=Proteins).

523 Protein disorderness was predicted based on amino acid sequences using PrDOS
524 (http://prdos.hgc.jp/cgi-bin/top.cgi) with the default setting[68].

525 Gene expression correlation was analyzed with AtCAST3.1 using default settings
526 (http://atpbsmd.yokohama-cu.ac.jp/cgi/atcast/home.cgi)[33].

RNA sequencing and data analysis

RNA was extracted from 14-day-old wild-type and *acinus-2 pinin-1* seedlings using RNeasy mini kit (Qiagen) and treated with TURBO DNA-free Kit (Ambion) to remove any genomic DNA contamination. The mRNA libraries were constructed using NEBNext RNA Library Prep Kit for Illumina following the standard Illumina protocol. Illumina sequencing was performed in the Sequencing Center for Personalized Medicine, Department of Genetics in Stanford University using an Illumina HiSeq 2000 System. The RNA-seq data have been deposited at the NCBI Gene Expression Omnibus (GEO) database under the accession number GSE110923.

Differential gene expression was analyzed using STAR and Deseq2. Trimmed and quality control-filtered sequence reads were mapped to the *Arabidopsis* reference genome (TAIR10) using STAR (v.2.54) in two pass mode (parameters: –outFilterScoreMinOverLread 0.3, –outFilterMatchNminOverLread 0.3, –outSAMstrandField intronMotif, –outFilterType BySJout, –outFilterIntronMotifs RemoveNoncanonical, –quantMode TranscriptomeSAM GeneCounts)[69]. To obtain uniquely mapping reads, these were filtered by mapping quality (q20), and PCR duplicates were removed using Samtools rmdup (v.1.3.1). Gene expression was analyzed in R (v.3.4.1) using DEseq2 (v.1.16.1)[70]. Significant differentially expressed genes are selected based on adjP-value<0.02 and fold change >2.

Alternative splicing analysis was performed with RACKJ using default setting (online manual available at http://rackj.sourceforge.net/)[71]. Raw intron retention data was analyzed and filtered to reduce false positives with 2 criteria: 1) fold change of intron retention >2, p-value<0.05 in a two-tail T-test and 2) Intron RPKM>1 and estimated percentage of IR >5% in the sample that shows increased IR in the intron. Raw exon skipping (ES) data was analyzed and filtered with 2 criteria: 1) fold change of ES rate>2, p-value<0.05 in a two-tail T-test, and 2) Increased ES event is supported by reads with RPKM>1 and ES rate>5%. For alternative donor/acceptor usage discovery, only events that appear significantly different in each pair-wise comparison between wild-type and *acinus-2 pinin-1* (fisher's exact test p-value<0.05) were considered significant and were further filtered with 2 criteria: 1) fold change >2, and 2) Increased alternative donor/acceptor usage is supported by reads with RPKM>1 and rate>5%.

RNA extraction, reverse transcription PCR

RNA was extracted from seedlings using Spectrum™ Plant Total RNA Kit (Sigma) and treated with TURBO DNA-free Kit (Ambion) to remove any genomic DNA contaminants. Purified

RNA (500ng) is subjected to cDNA synthesis using RevertAid Reverse Transcriptase (Thermo) with Oligo(dT)$_{18}$ primer. The synthesized cDNA was used for PCR and qPCR analyses. PCR products were analyzed by gel electrophoresis and the PCR band intensities were quantified using ImageJ. The qPCR analyses were performed with the SensiMix™ SYBR® & Fluorescein Kit (Bioline) on a LightCycler 480 (Roches). For each sample, 2 technical replicates were performed. The comparative cycle threshold method was used for calculating transcript level. Primers used for *FLC* antisense analysis are the same as in previous publication[37].Sequences of oligo primers are listed in Supplementary data 4.

RNA immunoprecipitation

RNA immunoprecipitation (RNA-IP) was performed using a protocol modified based on published procedures[22]. Briefly, 3 grams of tissues of 7-day-old *35S::AtACINUS-GFP/acinus-2* and *35S::GFP* seedlings were cross-linked with 1% (v/v) formaldehyde for 15 mins. Cross-linked RNA-protein complexes were extracted in NLB buffer (20 mmol/L Tris-HCl, pH 8.0, 150 mmol/L NaCl, 2 mmol/L EDTA, 1% (v/v) Triton X-100, 0.1% (w/v) SDS, 1 mmol/L PMSF and 2X Protease Inhibitor (Roche)) and sheared by sonication (25% amplitude, 0.5''on/0.5''off for 2minX3 cycles on a Branson Digital Sonifier). Immunoprecipitation was carried out with Protein A magnetic beads (Thermo Fisher) that were pre-incubated overnight with homemade anti-GFP antibody (5 µg for each sample) for 1 hr on a rotator. Beads were washed 5 times with 1ml NLB buffer (no SDS, 0.5% (v/v) Triton X-100) with 80 U/ml RNase inhibitor. To elute the immuno-complex, 100ul Elution Buffer (20 mmol/L Tris-HCl, pH 8.0, 10 mmol/L EDTA, 1% (w/v) SDS, 800U/ml RNase inhibitor) was added to the beads and incubated at 65 ^{o}C for 15 mins. The elute was incubated with1ul 20 mg/ml Protease K at 65 ^{o}C for 1hr for protein digestion and reverse-crosslinking. RNA was purified and concentrated using the RNA Clean & Concentrator™ kit (Zymo). On-column DNase digestion was performed to remove DNA contaminations. Samples were kept on ice whenever possible during the experiment. Three biological replicates were performed and the co-immunoprecipitated *ABH1* transcripts were quantified with RT-qPCR, and the results were normalized to 25S rRNA[72].

ChIP-PCR

Chromatin immunoprecipitation (ChIP) analysis was performed using a similar protocol to previous publications[73]. Briefly, tissue crosslinking, protein extraction, and immunoprecipitation were carried out as described above for RNA-IP. The beads were washed with low-salt buffer (50 mmol/L Tris-HCl at pH 8.0, 2 mmol/L EDTA, 150 mmol/L NaCl and 0.5%

(v/v) Triton X-100), high-salt buffer (50 mmol/L Tris-HCl at pH 8.0, 2 mmol/L EDTA, 500 mmol/L NaCl and 0.5% (v/v) Triton X-100), LiCl buffer (10 mmol/L Tris-HCl at pH 8.0, 1 mmol/L EDTA, 0.25 mol/L LiCl, 0.5% (w/v) NP-40 and 0.5% (w/v) sodium deoxycholate) and TE buffer (10 mmol/L Tris-HCl at pH 8.0 and 1 mmol/L EDTA), and eluted with elution buffer (1% (w/v) SDS and 0.1 mmol/L $NaHCO_3$). After reverse cross-linking and proteinase K digestion, the DNA was purified with a PCR purification kit (Thermol Fisher) and analyzed by PCR. Three biological replicates were performed. *FLC* primers were based on previous publications[47].

SILIA-MS quantitative analysis of the AtACINUS interactome

Stable-isotope-labeling in *Arabidopsis* mass spectrometry (SILIA-MS) was used for quantitative analysis of the AtACINUS interactome. The WT and *acinus-2* plants were grown for two weeks at 21°C under constant light on vertical plates of ^{14}N or ^{15}N medium (Hogland's No. 2 salt mixture without nitrogen 1.34g/L, 6g/L phytoblend, 2 µmol/L propiconazole, and 1g/L KNO_3 or 1g/L $K^{15}NO_3$ (Cambridge Isotope Laboratories), pH5.8). About 5 g of tissue was harvested for each sample, ground in liquid nitrogen and stored in -80°C. Immunoprecipitation was performed as described previously with slight modifications[74]. Briefly, proteins were extracted in 10 mL MOPS buffer (100 mmol/L MOPS, pH 7.6, 150 mmol/L NaCl, 1% (v/v) TritonX-100, 1 mmol/L phenylmethylsulfonyl fluoride (PMSF), 2X Complete protease inhibitor cocktail, and PhosStop cocktail (Roche)), centrifuged, and filtered through two layers of Miracloth. The flow through was incubated with 20 µg anti-AtACINUS antibody for one hour at 4 °C, then 50 µL protein A agarose beads were added and incubated for another hour, followed by four 2-min washes with immunoprecipitation buffer. At the last wash, ^{14}N-labeled Wild-type and ^{15}N-labeld *acinus-2* IP samples or reciprocal ^{15}N-labeled Wild-type and ^{14}N-labeled *acinus-2* IP samples were mixed, and eluted with 2x SDS buffer. The eluted proteins were separated by SDS-PAGE. After Coomassie Brillant blue staining, the whole lane of protein samples was excised in ten segments and subjected to in-gel digestion with trypsin.

The peptide mixtures were desalted using C18 ZipTips (Millipore) and analyzed on a LTQ-Orbitrap Velos mass spectrometer (Thermo Fisher), equipped with a NanoAcquity liquid chromatography system (Waters). Peptides were loaded onto a trapping column (NanoAcquity UPLC 180 µm X 20 mm; Waters) and then washed with 0.1% (v/v) formic acid. The analytical column was a BEH130 C18 100 µm X 100 mm (Waters). The flow rate was 600 nL/min. Peptides were eluted by a gradient from 2-30% solvent B (100% (v/v) acetonitrile/ 0.1% (v/v) formic acid) over 34 min, followed by a short wash at 50% solvent B. After a precursor scan was measured in the Orbitrap by scanning from mass-to-charge ratio 350 to 1500, the six most

intense multiply charged precursors were selected for collision-induced dissociation in the linear ion trap.

Tandem mass spectrometry peak lists were extracted using an in-house script PAVA, and data were searched using Protein Prospector against the *Arabidopsis* Information Resource (TAIR10) database, to which reverse sequence versions were concatenated (a total of 35,386 entries) to allow estimation of a false discovery rate (FDR). Carbamidomethyl cysteine was searched as a fixed modification and oxidation of methionine and N-terminal acetylation as variable modifications. Data were searched with a 10 ppm tolerance for precursor ion and 0.6 Da for fragment ions. Peptide and protein FDRs were set as 0.01 and 0.05. ^{15}N labeled amino acids were also searched as a fixed modification for ^{15}N data. ^{15}N labeling efficiency was calculated as about 96%, by manually comparing experimental peak envelop data of the ^{15}N labeled peptide from top 10 proteins in the raw data to theoretical isotope distributions using Software Protein-prospector (MS-Isotope app). Quantification was done using Protein Prospector which automatically adjusts the L/H ratio with labeling efficiency. The SILIA ratio (WT/*acinus-2*) was normalized using the average ratios of non-specific interactor ribosomal proteins (with more than five peptides). ^{15}N labeling samples in general have less identification rates of proteins because of 96% labeling efficiency. The data has been deposited to PRIDE with project accession: PXD020700.

Label-free mass spectrometric analysis of AtACINUS and its interactome

The *AtACINUS-GFP*/*acinus-2* and TAP-GFP seedlings[38] were grown for 7 days at 21°C under constant light on ½ MS medium. Tissues were harvested, ground in liquid nitrogen and stored in -80°C.

Immunoprecipitation was performed as described previously with slight modifications [74]. Briefly, proteins were extracted in MOPS buffer (100 mmol/L MOPS, pH 7.6, 150 mmol/L NaCl, 1% (v/v) TritonX-100, 1 mmol/L phenylmethylsulfonyl fluoride (PMSF), 2X Complete protease inhibitor cocktail, and PhosStop cocktail (Roche) and 20 µmol/L PUGNAc inhibitor (Sigma), centrifuged, and filtered through two layers of Miracloth, then incubated with a modified version of LaG16-LaG2 anti-GFP nanobody[75] conjugated to dynabeads (Invitrogen), for 3 hr at 4°C, followed by four 2-min washes with immunoprecipitation buffer and eluted with 2% (w/v) SDS buffer containing 10 mmol/L tris(2-carboxyethyl) phosphine (TCEP) and 40 mmol/L chloroacetamide at 95°C for 5 mins. The eluted proteins were separated by SDS-PAGE. After

Colloidal blue staining, the whole lane of protein samples was excised in two segments and subjected to in-gel digestion with trypsin. Three biological experiments were performed.

The peptide mixtures were desalted using C18 ZipTips (Millipore) and analyzed on a Q-Exactive HF hybrid quadrupole-Orbitrap mass spectrometer (Thermo Fisher) equipped with an Easy LC 1200 UPLC liquid chromatography system (Thermo Fisher). Peptides were separated using analytical column ES803 (Thermo Fisher). The flow rate was 300nL/min and a 120-min gradient was used. Peptides were eluted by a gradient from 3 to 28% solvent B (80% (v/v) acetonitrile/0.1% (v/v) formic acid) over 100 mins and from 28 to 44% solvent B over 20 mins, followed by short wash at 90% solvent B. Precursor scan was from mass-to-charge ratio (*m/z*) 375 to1600 and top 20 most intense multiply charged precursor were selection for fragmentation. Peptides were fragmented with higher-energy collision dissociation (HCD) with normalized collision energy (NCE) 27.

The raw data were processed by MaxQuant using most of preconfigured settings[76]. The search was against the same TAIR database as mentioned above. Carbamidomethylcysteine was searched as a fixed modification and oxidation of methionine and N-terminal acetylation as variable modifications. Data were searched with a 4.5ppm tolerance for precursor ion and 20 ppm for fragment ions. The second peptide feature was enabled. A maximum of two missed cleavages was allowed. Peptide and protein FDRs were set as 0.01. Minimum required peptide length was seven amino acids. Multiplicity was set to 1. Label-free quantification (LFQ) was enabled. The match between runs option was enabled with a match time window of 0.7 min and alignment time window as 20 mins. Quantification was done on unique and razor peptides and a minimum ratio count was set to 2.

The proteinGroups.txt generated by MaxQuant were loaded to Perseus[77]. The results were filtered by removing identified proteins by only modified sites, or hits to reverse database and contaminants. LFQ intensity values were logarithmized. The pull-downs were divided to AtACINUS-GFP and TAP-GFP control. Samples were grouped in triplicates and identifications were filtered for proteins having at least three values in at least one replicate group. Signals that were originally zero were imputed with random numbers from a normal distribution (width 0.3, shift =1.8). Volcano plot was performed with x axis representing the logarithmic ratios of protein intensities between AtACINUS-GFP and TAP-GFP. The hyperbolic curve that separates AtACINUS specific interactor from background was drawn using threshold value FDR 0.01 and curve bend S0 value 2.

LFQ data and SILIA data were combined and filtered to get a high-confidence list of interactors: 1) Significant enrichment in LFQ three biological replicates (FDR=0.01, S0=2); 2) Enrichment of over 2 folds in both SILIA biological experiment; or over 2 folds in one SILIA experiment, but not identified in second SILIA experiment. If the proteins are only identified and quantified by LFQ three biological replicates, then a higher stringency cut off (enrichment> 16 fold, t test >4) is used. The data was deposited to PRIDE with project accession: PXD020748.

For affinity purification of AtACINUS using *in vivo* biotinylation, the *acinus pinin* mutant was transformed with a T-DNA construct that expresses AtACINUS as a fusion with TurboID from the 35S promoter[65]. The *AtACINUS-YFP-TurboID*/*acinus-2 pinin-1* seedlings were treated with 0 or 50 µmmol/L biotin for 3 hours. The AtACINUS-YFP-Turbo protein was affinity purified using streptavidin beads as previously described[65] using a modified extraction buffer containing 20 µmol/L PUGNAC and 1 x PhosphoStop. After on-bead tryptic digestion, the samples were analyzed as described above in the label-free IP-MS section on a Q-Exactive HF instrument. Data were searched as described above but allowing additional modifications: O-GlcNAcylation modification on S/T and neutral loss, O-fucosylation on S/T and neutral loss, phosphorylation on S/T and biotinylation on lysine. The data was deposited to PRIDE with accession number: PXD020749.

Targeted quantification comparing wild-type and the *acinus-2 pinin-1* double mutant

The wild-type and *acinus-2 pinin-1* plants were grown Hoagland medium containing ^{14}N or ^{15}N (1.34g/L Hogland's No2 salt mixture without nitrogen, 6g/L phytoblend, and 1g/L KNO_3 or 1g/L $K^{15}NO_3$ (Cambridge Isotope Laboratories), pH5.8). Proteins were extracted from 6 samples (one ^{14}N-labelled Col, two of ^{15}N-labelled Col, two of ^{14}N-labelled *acinus-2 pinin-1* and one ^{15}N-labelled *acinus-2 pinin-1)* individually using SDS sample buffer and mixed as the followings: one forward sample F1 (^{14}N Col/ ^{15}N *acinus-2 pinin-1*) and two reverse samples R2 and R3 (^{14}N *acinus-2 pinin-1*/^{15}N Col) and separated by the SDS-PAGE gel with a very short run. Two segments (upper part (U) ranging from the loading well to ~ 50KD; lower part (L) ranging from ~ 50KD to the dye front) were excised, trypsin digested and analyzed by liquid chromatography mass spectrometry (LC-MS) as described above in the label-free IP-MS section on a Q-Exactive HF instrument using an ES803A analytical column. Data-dependent acquisition was used first to get the peptide information from multiple proteins with peptide mass/charge (*m/z*), retention time and MS2 fragments. PININ peptide information was from an IP-MS experiment. For targeted analysis, parallel reaction monitoring (PRM) acquisition[78] using a 20 min window was scheduled with an orbitrap resolution at 60,000, AGC value 2e5 and maximum fill time of

200 ms. The isolation window for each precursor was set at 1.4 *m/z* unit. Data processing was similar to the previous report[79] with a 5 ppm window using skyline from ^{14}N- and ^{15}N -labeled samples. Peak areas of fragments were calculated from each sample, the sum of peak areas from upper segment and lower segment was used to calculate *acinus-2 pinin-1*/Col ratios for each peptide, normalized to TUBULIN2 to get the normalized ratios. Median number of multiple ratio measurements is used for each protein.

Data Availability

Proteomic Data that support the findings of this study have been deposited in Proteomics Identification Database (PRIDE) with the accession codes: PXD020700, PXD020748, PXD020749. The RNA-seq data that support the findings of this study have been deposited in the National Center for Biotechnology Information Gene Expression Ominbus and are accessible through the GEO series accession number GSE110923. All other related data are available from the corresponding authors upon request.

Supplementary information

Supplementary Figures 1-16

Supplementary data 1: Summary of reads mapping quality and differentially expressed genes in *acinus-2 pinin-1* identified by RNA-seq analysis.

Supplementary data 2: Alternative splicing events in *acinus-2 pinin-1* identified by RNA-seq analysis.

Supplementary data 3: AtACINUS interactome.

Supplementary data 4: List of primers used in the study.

Supplementary data 5: Targeted quantification on AtACINUS, AtPININ, SR45 and AtSAP18 between Col and *acinus-2 pinin-1* mutant.

Acknowledgments:

We thank Jeffrey Mugridge and John D Gross for technical assistance. We thank Brian Chait and Michael Rout labs for the LaG16-LaG2 construct and thank Dr. Jixian Zhai for providing the *Arabidopsis* pts intron dataset. We also thank the Salk Institute and *Arabidopsis* Biological Resource Center for the *Arabidopsis* T-DNA insertion lines. This work was supported by National Institutes of Health (NIH) (5R01GM066258 to Z-Y.W., R01GM135706 to S.L.X.,

749 8P41GM103481 to A.L.B., and 2R01GM047475 to P.H.Q) and the Carnegie endowment fund to
750 the Carnegie mass spectrometry facility.

751 **Author Contributions:**

752 Z.D., K.L, J.O, and A.L.B. identified AtACINUS; Z.D., S.L.X., and S.P. analyzed the *acinus*
753 mutant; Y.B., S.L.X. and D.S. characterized the *acinus pinin* double mutants; Y.B performed
754 RNA-seq and T.H helped with data analysis; W.N. performed proteomic analysis of AtACINUS
755 interactome under supervision by A.L.B., P.H.Q and S.L.X. R.S performed targeted
756 quantification, S.H. performed affinity purification of biotinylated protein and R.S prepared
757 spectra. Z-Y.W and S.L.X conceived the projects; Y.B., S.L.X. and Z-Y.W. wrote the manuscript.

758 **Competing financial interests:** The authors declare no competing financial interests.

759

760 References

761 1 Hanover, J. A., Krause, M. W. & Love, D. C. The hexosamine signaling pathway: O-GlcNAc cycling
762 in feast or famine. *Biochim Biophys Acta* **1800**, 80-95, doi:10.1016/j.bbagen.2009.07.017 (2010).
763 2 Hart, G. W., Slawson, C., Ramirez-Correa, G. & Lagerlof, O. Cross Talk Between O-GlcNAcylation
764 and Phosphorylation: Roles in Signaling, Transcription, and Chronic Disease. *Annual Review of*
765 *Biochemistry, Vol 80* **80**, 825-858, doi:10.1146/annurev-biochem-060608-102511 (2011).
766 3 Ma, J. & Hart, G. W. O-GlcNAc profiling: from proteins to proteomes. *Clin Proteomics* **11**, 8,
767 doi:10.1186/1559-0275-11-8 (2014).
768 4 Yang, X. & Qian, K. Protein O-GlcNAcylation: emerging mechanisms and functions. *Nat Rev Mol*
769 *Cell Biol* **18**, 452-465, doi:10.1038/nrm.2017.22 (2017).
770 5 Chen, P. H., Chi, J. T. & Boyce, M. Functional crosstalk among oxidative stress and O-GlcNAc
771 signaling pathways. *Glycobiology* **28**, 556-564, doi:10.1093/glycob/cwy027 (2018).
772 6 Banerjee, P. S., Lagerlof, O. & Hart, G. W. Roles of O-GlcNAc in chronic diseases of aging. *Mol*
773 *Aspects Med* **51**, 1-15, doi:10.1016/j.mam.2016.05.005 (2016).
774 7 Jacobsen, S. E. & Olszewski, N. E. Mutations at the SPINDLY locus of Arabidopsis alter gibberellin
775 signal transduction. *Plant Cell* **5**, 887-896, doi:10.1105/tpc.5.8.887 (1993).
776 8 Liang, L. *et al.* SPINDLY is involved in ABA signaling bypassing the PYR/PYLs/RCARs-mediated
777 pathway and partly through functional ABAR. *Environmental and Experimental Botany* **151**, 43-
778 54 (2018).
779 9 Hartweck, L. M., Scott, C. L. & Olszewski, N. E. Two O-linked N-acetylglucosamine transferase
780 genes of Arabidopsis thaliana L. Heynh. have overlapping functions necessary for gamete and
781 seed development. *Genetics* **161**, 1279-1291 (2002).
782 10 Zentella, R. *et al.* The Arabidopsis O-fucosyltransferase SPINDLY activates nuclear growth
783 repressor DELLA. *Nat Chem Biol* **13**, 479-485, doi:10.1038/nchembio.2320 (2017).
784 11 Zentella, R. *et al.* O-GlcNAcylation of master growth repressor DELLA by SECRET AGENT
785 modulates multiple signaling pathways in Arabidopsis. *Genes Dev* **30**, 164-176,
786 doi:10.1101/gad.270587.115 (2016).

12 Olszewski, N. E., West, C. M., Sassi, S. O. & Hartweck, L. M. O-GlcNAc protein modification in plants: Evolution and function. *Biochim Biophys Acta* **1800**, 49-56, doi:10.1016/j.bbagen.2009.11.016 (2010).

13 Xu, S. L. *et al.* Proteomic analysis reveals O-GlcNAc modification on proteins with key regulatory functions in Arabidopsis. *Proc Natl Acad Sci U S A* **114**, E1536-E1543, doi:10.1073/pnas.1610452114 (2017).

14 Murachelli, A. G., Ebert, J., Basquin, C., Le Hir, H. & Conti, E. The structure of the ASAP core complex reveals the existence of a Pinin-containing PSAP complex. *Nat Struct Mol Biol* **19**, 378-386, doi:10.1038/nsmb.2242 (2012).

15 Wang, Z., Ballut, L., Barbosa, I. & Le Hir, H. Exon Junction Complexes can have distinct functional flavours to regulate specific splicing events. *Sci Rep* **8**, 9509, doi:10.1038/s41598-018-27826-y (2018).

16 Schwerk, C. *et al.* ASAP, a Novel Protein Complex Involved in RNA Processing and Apoptosis. *Molecular and Cellular Biology* **23**, 2981-2990, doi:10.1128/mcb.23.8.2981-2990.2003 (2003).

17 Deka, B. & Singh, K. K. Multifaceted Regulation of Gene Expression by the Apoptosis- and Splicing-Associated Protein Complex and Its Components. *Int J Biol Sci* **13**, 545-560, doi:10.7150/ijbs.18649 (2017).

18 Carvalho, R. F., Carvalho, S. D. & Duque, P. The plant-specific SR45 protein negatively regulates glucose and ABA signaling during early seedling development in Arabidopsis. *Plant Physiol* **154**, 772-783, doi:10.1104/pp.110.155523 (2010).

19 Ali, G. S. *et al.* Regulation of plant developmental processes by a novel splicing factor. *PLoS One* **2**, e471, doi:10.1371/journal.pone.0000471 (2007).

20 Ausin, I., Greenberg, M. V., Li, C. F. & Jacobsen, S. E. The splicing factor SR45 affects the RNA-directed DNA methylation pathway in Arabidopsis. *Epigenetics* **7**, 29-33, doi:10.4161/epi.7.1.18782 (2012).

21 Zhang, X. N. *et al.* Transcriptome analyses reveal SR45 to be a neutral splicing regulator and a suppressor of innate immunity in Arabidopsis thaliana. *BMC Genomics* **18**, 772, doi:10.1186/s12864-017-4183-7 (2017).

22 Xing, D., Wang, Y., Hamilton, M., Ben-Hur, A. & Reddy, A. S. Transcriptome-Wide Identification of RNA Targets of Arabidopsis SERINE/ARGININE-RICH45 Uncovers the Unexpected Roles of This RNA Binding Protein in RNA Processing. *Plant Cell* **27**, 3294-3308, doi:10.1105/tpc.15.00641 (2015).

23 Chen, S. L. *et al.* Quantitative Proteomics Reveals a Role for SERINE/ARGININE-Rich 45 in Regulating RNA Metabolism and Modulating Transcriptional Suppression via the ASAP Complex in Arabidopsis thaliana. *Front Plant Sci* **10**, 1116, doi:10.3389/fpls.2019.01116 (2019).

24 Hill, K., Wang, H. & Perry, S. E. A transcriptional repression motif in the MADS factor AGL15 is involved in recruitment of histone deacetylase complex components. *Plant J* **53**, 172-185, doi:10.1111/j.1365-313X.2007.03336.x (2008).

25 Song, C. P. & Galbraith, D. W. AtSAP18, an orthologue of human SAP18, is involved in the regulation of salt stress and mediates transcriptional repression in Arabidopsis. *Plant Mol Biol* **60**, 241-257, doi:10.1007/s11103-005-3880-9 (2006).

26 Questa, J. I., Song, J., Geraldo, N., An, H. L. & Dean, C. Arabidopsis transcriptional repressor VAL1 triggers Polycomb silencing at FLC during vernalization. *Science* **353**, 485-488, doi:10.1126/science.aaf7354 (2016).

27 Aravind, L. & Koonin, E. V. SAP - a putative DNA-binding motif involved in chromosomal organization. *Trends Biochem Sci* **25**, 112-114, doi:10.1016/s0968-0004(99)01537-6 (2000).

28 Whittaker, C. & Dean, C. The FLC Locus: A Platform for Discoveries in Epigenetics and Adaptation. *Annu Rev Cell Dev Biol* **33**, 555-575, doi:10.1146/annurev-cellbio-100616-060546 (2017).

29 Shaul, O. Unique Aspects of Plant Nonsense-Mediated mRNA Decay. *Trends Plant Sci* **20**, 767-779, doi:10.1016/j.tplants.2015.08.011 (2015).

30 Hugouvieux, V., Kwak, J. M. & Schroeder, J. I. An mRNA cap binding protein, ABH1, modulates early abscisic acid signal transduction in Arabidopsis. *Cell* **106**, 477-487 (2001).

31 Hugouvieux, V. *et al.* Localization, ion channel regulation, and genetic interactions during abscisic acid signaling of the nuclear mRNA cap-binding protein, ABH1. *Plant Physiol* **130**, 1276-1287, doi:10.1104/pp.009480 (2002).

32 Kuhn, J. M., Hugouvieux, V. & Schroeder, J. I. mRNA cap binding proteins: effects on abscisic acid signal transduction, mRNA processing, and microarray analyses. *Curr Top Microbiol Immunol* **326**, 139-150 (2008).

33 Kakei, Y. & Shimada, Y. AtCAST3.0 update: a web-based tool for analysis of transcriptome data by searching similarities in gene expression profiles. *Plant Cell Physiol* **56**, e7, doi:10.1093/pcp/pcu174 (2015).

34 Wang, Z. *et al.* ABA signalling is fine-tuned by antagonistic HAB1 variants. *Nat Commun* **6**, 8138, doi:10.1038/ncomms9138 (2015).

35 Zhan, X. *et al.* An Arabidopsis PWI and RRM motif-containing protein is critical for pre-mRNA splicing and ABA responses. *Nat Commun* **6**, 8139, doi:10.1038/ncomms9139 (2015).

36 Liu, F., Marquardt, S., Lister, C., Swiezewski, S. & Dean, C. Targeted 3' processing of antisense transcripts triggers Arabidopsis FLC chromatin silencing. *Science* **327**, 94-97, doi:10.1126/science.1180278 (2010).

37 Marquardt, S. *et al.* Functional consequences of splicing of the antisense transcript COOLAIR on FLC transcription. *Mol Cell* **54**, 156-165, doi:10.1016/j.molcel.2014.03.026 (2014).

38 Shen, H. *et al.* Light-induced phosphorylation and degradation of the negative regulator PHYTOCHROME-INTERACTING FACTOR1 from Arabidopsis depend upon its direct physical interactions with photoactivated phytochromes. *Plant Cell* **20**, 1586-1602, doi:10.1105/tpc.108.060020 (2008).

39 Hogg, R., McGrail, J. C. & O'Keefe, R. T. The function of the NineTeen Complex (NTC) in regulating spliceosome conformations and fidelity during pre-mRNA splicing. *Biochem Soc Trans* **38**, 1110-1115, doi:10.1042/BST0381110 (2010).

40 Monaghan, J. *et al.* Two Prp19-like U-box proteins in the MOS4-associated complex play redundant roles in plant innate immunity. *PLoS Pathog* **5**, e1000526, doi:10.1371/journal.ppat.1000526 (2009).

41 Koncz, C., Dejong, F., Villacorta, N., Szakonyi, D. & Koncz, Z. The spliceosome-activating complex: molecular mechanisms underlying the function of a pleiotropic regulator. *Front Plant Sci* **3**, 9, doi:10.3389/fpls.2012.00009 (2012).

42 Reichow, S. L., Hamma, T., Ferre-D'Amare, A. R. & Varani, G. The structure and function of small nucleolar ribonucleoproteins. *Nucleic Acids Res* **35**, 1452-1464, doi:10.1093/nar/gkl1172 (2007).

43 Boehm, V. & Gehring, N. H. Exon Junction Complexes: Supervising the Gene Expression Assembly Line. *Trends Genet* **32**, 724-735, doi:10.1016/j.tig.2016.09.003 (2016).

44 Le Hir, H., Sauliere, J. & Wang, Z. The exon junction complex as a node of post-transcriptional networks. *Nat Rev Mol Cell Biol* **17**, 41-54, doi:10.1038/nrm.2015.7 (2016).

45 Woodward, L. A., Mabin, J. W., Gangras, P. & Singh, G. The exon junction complex: a lifelong guardian of mRNA fate. *Wiley Interdiscip Rev RNA* **8**, doi:10.1002/wrna.1411 (2017).

46 Mahrez, W. *et al.* BRR2a Affects Flowering Time via FLC Splicing. *PLoS Genet* **12**, e1005924, doi:10.1371/journal.pgen.1005924 (2016).

47 He, Y., Doyle, M. R. & Amasino, R. M. PAF1-complex-mediated histone methylation of FLOWERING LOCUS C chromatin is required for the vernalization-responsive, winter-annual habit in Arabidopsis. *Genes Dev* **18**, 2774-2784, doi:10.1101/gad.1244504 (2004).

48 Rodor, J., Pan, Q., Blencowe, B. J., Eyras, E. & Caceres, J. F. The RNA-binding profile of Acinus, a peripheral component of the exon junction complex, reveals its role in splicing regulation. *RNA* **22**, 1411-1426, doi:10.1261/rna.057158.116 (2016).

49 Vucetic, Z. *et al.* Acinus-S' represses retinoic acid receptor (RAR)-regulated gene expression through interaction with the B domains of RARs. *Mol Cell Biol* **28**, 2549-2558, doi:10.1128/MCB.01199-07 (2008).

50 Wang, F., Soprano, K. J. & Soprano, D. R. Role of Acinus in regulating retinoic acid-responsive gene pre-mRNA splicing. *J Cell Physiol* **230**, 791-801, doi:10.1002/jcp.24804 (2015).

51 Akin, D., Newman, J. R., McIntyre, L. M. & Sugrue, S. P. RNA-seq analysis of impact of PNN on gene expression and alternative splicing in corneal epithelial cells. *Mol Vis* **22**, 40-60 (2016).

52 Pieczynski, M. *et al.* Down-regulation of CBP80 gene expression as a strategy to engineer a drought-tolerant potato. *Plant Biotechnol J* **11**, 459-469, doi:10.1111/pbi.12032 (2013).

53 Saez, A. *et al.* Gain-of-function and loss-of-function phenotypes of the protein phosphatase 2CHAB1reveal its role as a negative regulator of abscisic acid signalling. *The Plant Journal* **37**, 354-369, doi:10.1046/j.1365-313X.2003.01966.x (2004).

54 Vlad, F. *et al.* Protein phosphatases 2C regulate the activation of the Snf1-related kinase OST1 by abscisic acid in Arabidopsis. *Plant Cell* **21**, 3170-3184, doi:10.1105/tpc.109.069179 (2009).

55 Carvalho, R. F. *et al.* The Arabidopsis SR45 Splicing Factor, a Negative Regulator of Sugar Signaling, Modulates SNF1-Related Protein Kinase 1 Stability. *Plant Cell* **28**, 1910-1925, doi:10.1105/tpc.16.00301 (2016).

56 Liu, Y. *et al.* Identification of the Arabidopsis REDUCED DORMANCY 2 gene uncovers a role for the polymerase associated factor 1 complex in seed dormancy. *PLoS One* **6**, e22241, doi:10.1371/journal.pone.0022241 (2011).

57 Tange, T. O., Shibuya, T., Jurica, M. S. & Moore, M. J. Biochemical analysis of the EJC reveals two new factors and a stable tetrameric protein core. *RNA* **11**, 1869-1883, doi:10.1261/rna.2155905 (2005).

58 Oldfield, C. J. & Dunker, A. K. Intrinsically disordered proteins and intrinsically disordered protein regions. *Annu Rev Biochem* **83**, 553-584, doi:10.1146/annurev-biochem-072711-164947 (2014).

59 Swain, S. M., Tseng, T. S. & Olszewski, N. E. Altered expression of SPINDLY affects gibberellin response and plant development. *Plant Physiol* **126**, 1174-1185 (2001).

60 Xing, L. *et al.* Arabidopsis O-GlcNAc transferase SEC activates histone methyltransferase ATX1 to regulate flowering. *EMBO J* **37**, doi:10.15252/embj.201798115 (2018).

61 Tan, Z. W. *et al.* O-GlcNAc regulates gene expression by controlling detained intron splicing. *Nucleic Acids Res* **48**, 5656-5669, doi:10.1093/nar/gkaa263 (2020).

62 Boutz, P. L., Bhutkar, A. & Sharp, P. A. Detained introns are a novel, widespread class of post-transcriptionally spliced introns. *Genes Dev* **29**, 63-80, doi:10.1101/gad.247361.114 (2015).

63 Mauger, O., Lemoine, F. & Scheiffele, P. Targeted Intron Retention and Excision for Rapid Gene Regulation in Response to Neuronal Activity. *Neuron* **92**, 1266-1278, doi:10.1016/j.neuron.2016.11.032 (2016).

64 Jia, J. *et al.* Post-transcriptional splicing of nascent RNA contributes to widespread intron retention in plants. *Nat Plants* **6**, 780-788, doi:10.1038/s41477-020-0688-1 (2020).

65 Kim, T. W. *et al.* Application of TurboID-mediated proximity labeling for mapping a GSK3 kinase signaling network in Arabidopsis. *BioRxiv*, doi:10.1101/636324 (2019).

66 Li, W. *et al.* The EMBL-EBI bioinformatics web and programmatic tools framework. *Nucleic Acids Res* **43**, W580-584, doi:10.1093/nar/gkv279 (2015).

67 Edgar, R. C. MUSCLE: a multiple sequence alignment method with reduced time and space complexity. *Bmc Bioinformatics* **5**, 113, doi:10.1186/1471-2105-5-113 (2004).

68 Ishida, T. & Kinoshita, K. PrDOS: prediction of disordered protein regions from amino acid sequence. *Nucleic Acids Res* **35**, W460-464, doi:10.1093/nar/gkm363 (2007).
69 Dobin, A. *et al.* STAR: ultrafast universal RNA-seq aligner. *Bioinformatics* **29**, 15-21, doi:10.1093/bioinformatics/bts635 (2013).
70 Love, M. I., Huber, W. & Anders, S. Moderated estimation of fold change and dispersion for RNA-seq data with DESeq2. *Genome Biol* **15**, 550, doi:10.1186/s13059-014-0550-8 (2014).
71 Li, W., Lin, W. D., Ray, P., Lan, P. & Schmidt, W. Genome-wide detection of condition-sensitive alternative splicing in Arabidopsis roots. *Plant Physiol* **162**, 1750-1763, doi:10.1104/pp.113.217778 (2013).
72 Kojima, H. *et al.* Sugar-inducible expression of the nucleolin-1 gene of Arabidopsis thaliana and its role in ribosome synthesis, growth and development. *Plant Journal* **49**, 1053-1063, doi:10.1111/j.1365-313X.2006.03016.x (2007).
73 Oh, E., Zhu, J. Y. & Wang, Z. Y. Interaction between BZR1 and PIF4 integrates brassinosteroid and environmental responses. *Nat Cell Biol* **14**, 802-U864, doi:10.1038/ncb2545 (2012).
74 Ni, W. *et al.* Multisite light-induced phosphorylation of the transcription factor PIF3 is necessary for both its rapid degradation and concomitant negative feedback modulation of photoreceptor phyB levels in Arabidopsis. *Plant Cell* **25**, 2679-2698, doi:10.1105/tpc.113.112342 (2013).
75 Fridy, P. C. *et al.* A robust pipeline for rapid production of versatile nanobody repertoires. *Nat Methods* **11**, 1253-1260, doi:10.1038/nmeth.3170 (2014).
76 Cox, J. & Mann, M. MaxQuant enables high peptide identification rates, individualized p.p.b.-range mass accuracies and proteome-wide protein quantification. *Nature biotechnology* **26**, 1367-1372, doi:10.1038/nbt.1511 (2008).
77 Tyanova, S. *et al.* The Perseus computational platform for comprehensive analysis of (prote)omics data. *Nat Methods* **13**, 731-740, doi:10.1038/nmeth.3901 (2016).
78 Peterson, A. C., Russell, J. D., Bailey, D. J., Westphall, M. S. & Coon, J. J. Parallel reaction monitoring for high resolution and high mass accuracy quantitative, targeted proteomics. *Mol Cell Proteomics* **11**, 1475-1488, doi:10.1074/mcp.O112.020131 (2012).
79 Ni, W. *et al.* PPKs mediate direct signal transfer from phytochrome photoreceptors to transcription factor PIF3. *Nat Commun* **8**, 15236, doi:10.1038/ncomms15236 (2017).

Figure legends

Figure 1 | *AtACINUS* and *AtPININ* are genetically redundant. (**a**) Diagrams of the domain structures of AtACINUS and AtPININ. SAP: SAF-A/B, Acinus and PIAS motif. RRM: RNA-recognition motif. RSB: RNPS1-SAP18 binding domain. G and F indicates the position of O-GlcNAcylation and O-fucosylation modifications respectively. (**b**) The sequence alignment of the RSB domains of AtACINUS and AtPININ. Conserved amino acids are highlighted in green. (**c**) Diagrams of the AtACINUS and AtPININ (translation start at position 1) with T-DNA insertion sites in *acinus-1*, *acinus-2* and *pinin-1* mutants. (**d**) Plant morphologies of wild type (WT), *acinus-1*, *acinus-2, pinin-1*, *acinus-1 pinin-1* and *acinus-2 pinin-1* grown on soil for 20 days. (**e**) Five-week old WT, *acinus-1*, *acinus-2*, *pinin-1*, *acinus-1 pinin-1* and *acinus-2 pinin-1* plants grown under long day condition. Inset shows enlarged view of the *acinus*-1 *pinin-1* and *acinus-2 pinin-1* mutants. **(f)**

971 Expression of either AtACINUS-GFP or YFP-AtPININ suppresses the growth defects in
972 *acinus-2 pinin-1* double mutant (*ap*).

973 **Figure 2 | The *acinus pinin* double mutants showed ABA hypersensitive**
974 **phenotypes. (a,b)** Germination rates of wild-type, *acinus-2*, *pinin-1* and *acinus-2 pinin-*
975 *1* after different days on ½ MS medium without ABA (a) or with 0.25 µmol/L ABA (b). The
976 data points of wild-type, *acinus-2* and *pinin-1* overlap. **(c)** Seed germination rates of the
977 indicated genotypes on ½ MS medium supplemented with increasing concentrations of
978 ABA after five days. Note that the data points of *acinus-1 pinin-1* and *acinus-2 pinin-1*
979 overlap and those of wild-type, *acinus-1*, *acinus-2* and *pinin-1* overlap. **(d)** Seed
980 germination and development of the indicated genotypes on ½ MS medium with or
981 without 0.5 µmol/L ABA. The pictures were taken 6 days after germination. Error bars
982 indicate SD calculated from 3 biological replicates (n=3). Asterisks indicate significant
983 differences to wild type (two-sided Student's t-test, *P< 0.05, ** P< 0.01, *** P< 0.001).

984 **Figure 3 | RNA-sequencing analysis of *acinus-2 pinin-1* showed differential intron**
985 **retention and expression level of many genes.** (**a**) Number of introns that showed
986 increased or decreased intron retention in *acinus-2 pinin-1* and the number of genes
987 that contain these introns. (**b**) Comparison between genes differentially expressed in
988 *acinus-2 pinin-1* and ABA-responsive genes. RNA-seq was conducted using 14-day-old
989 light-grown seedlings for both genotypes.

990 **Figure 4 | *ABH1* and *HAB1* showed increased intron retention in *acinus-2 pinin-1***
991 **and *ABH1* and *HAB1* mRNAs are associated with AtACINUS.** (**a**) Integrative
992 genomic viewer (IGV) display of increased intron retention of the *ABH1* 10th intron in
993 *acinus-2 pinin-1* compared to WT. (**b**) RT-PCR of *ABH1* in 12-day-old seedlings of the
994 indicated genotypes using primers at positions indicated by arrowheads in panel (a). (**c**)
995 Intron retention ratio of *ABH1* 10th intron as determined by RT-qPCR in 12-day-old
996 seedlings of the indicated genotypes. The intron-containing form *ABH1.2* was highly
997 accumulated while the spliced form *ABH1.1* was reduced in *acinus-2 pinin-1* compared
998 to WT, the single mutants, or the double mutant complemented by *YFP-AtPININ* or
999 *AtACINUS-GFP.* (**d**) RT-PCR of *HAB1* in 12-day-old WT and *acinus-2 pinin-1* seedlings
1000 treated with ABA (100 µmol/L for 3 hrs). (**e**) RT-qPCR quantification of the fold changes

of expression levels of each splice forms of *HAB1* after ABA treatment of 12-day-old WT and *acinus-2 pinin-1* seedlings. (**f**,**g**)Quantification of *ABH1* and *HAB1* mRNAs by qPCR after RNA-IP using α-GFP antibody in 7-day-old *AtACINUS-GFP/acinus-2* seedlings, compared to *35S::GFP* as a negative control. Error bars in this figure indicate SD calculated from 3 biological replicates (n=3). Asterisks indicate significant differences to wild type or between indicated samples (two-sided Student's t-test, *P< 0.05, ** P< 0.01, *** P< 0.001).

Figure 5 | The *acinus-2 pinin-1* double mutant is late flowering with increased *FLC* expression. (**a**) Rosette leaf number of WT, *acinus-2*, *pinin-1* and *acinus-2 pinin-1* at bolting stage grown in long day condition. Error bars indicate SD calculated from n>12. (**b**) *FLC* expression level relative to *PP2a* in WT, *acinus-2*, *pinin-1* and *acinus-2 pinin-1,* determined by RT-qPCR in 12-day-old seedlings. Error bars indicate SD calculated from 3 biological replicates (n=3). (**c**) Analysis of AtACINUS-GFP association with the *FLC* locus by ChIP-PCR in 12-day-old *AtACINUS-GFP/acinus-2* seedlings. Wild type (WT) serves as the negative control. Bars below the gene structure diagram show regions analyze by PCR (blue bars indicate positive binding detected). GFP IP shows PCR products using immunoprecipitated DNA. *CO-FACTOR FOR NITRATE, REDUCTASE AND XANTHINE DEHYDROGENASE 5* (*CNX5*) serves as an internal control to show non-specific background DNA after immunoprecipitation. Asterisks indicate significant differences to wild type (two-sided Student's t-test, *P< 0.05, ** P< 0.01, *** P< 0.001).

Figure 6 | *A* subset of AtACINUS-dependent intron splicing events are affected in the *spy* and *sec* mutants. RT-PCR of *HAB1*, *EMB2247* and *TRM4D* in 7-day-old WT, *acinus-2 pinin*, *spy-t1*, *spy-4*, *sec-2* and *sec-5* seedlings with exon-spanning primers flanking the targeted introns.

Figure 7 | AtACINUS is O-GlcNAc and O-Fucose modified and associates with spliceosomal complexes, transcriptional regulators and chromatin remodeling proteins. (**a**) Diagram shows functional groups of AtACINUS-associated proteins. Proteins are grouped in boxes based on their association with known complexes or functions. Positive regulators of *FLC* are highlighted in red and negative regulators in blue. Seven-day-old seedlings were used for the label-free IP-MS experiments and 14-

day-old seedlings were used for the ^{15}N Stable-isotope-labeling in *Arabidopsis* (SILIA) quantitative MS experiments. (**b**,**c**) Higher energy collisional dissociation (HCD) mass spectra shows O-GlcNAcylation on Thr79 and a sequence spanning amino acid 400-423 of AtACINUS. The sequence ion series that retains this modification (shifted by 203Da) are labeled in blue (b). The sequence ion series that have lost the modification are labeled in red. HexNAc oxonium ion (*m/z* 204) and its fragments masses are labeled in red. (**d**) HCD spectrum shows O-fucosylation on a sequence spanning amino acid 169-197 of AtACINUS with neutral loss. (e) Proposed model of a molecular pathway in which nutrient sensing O-GlcNAcylation and O-fucosylation modulate the evolutionarily conserved RSB-domain protein AtACINUS, which controls transcription and alternative RNA splicing of specific target genes to modulate stress hormone sensitivity and developmental transitions such as seed germination and flowering in plants.

Fig.1

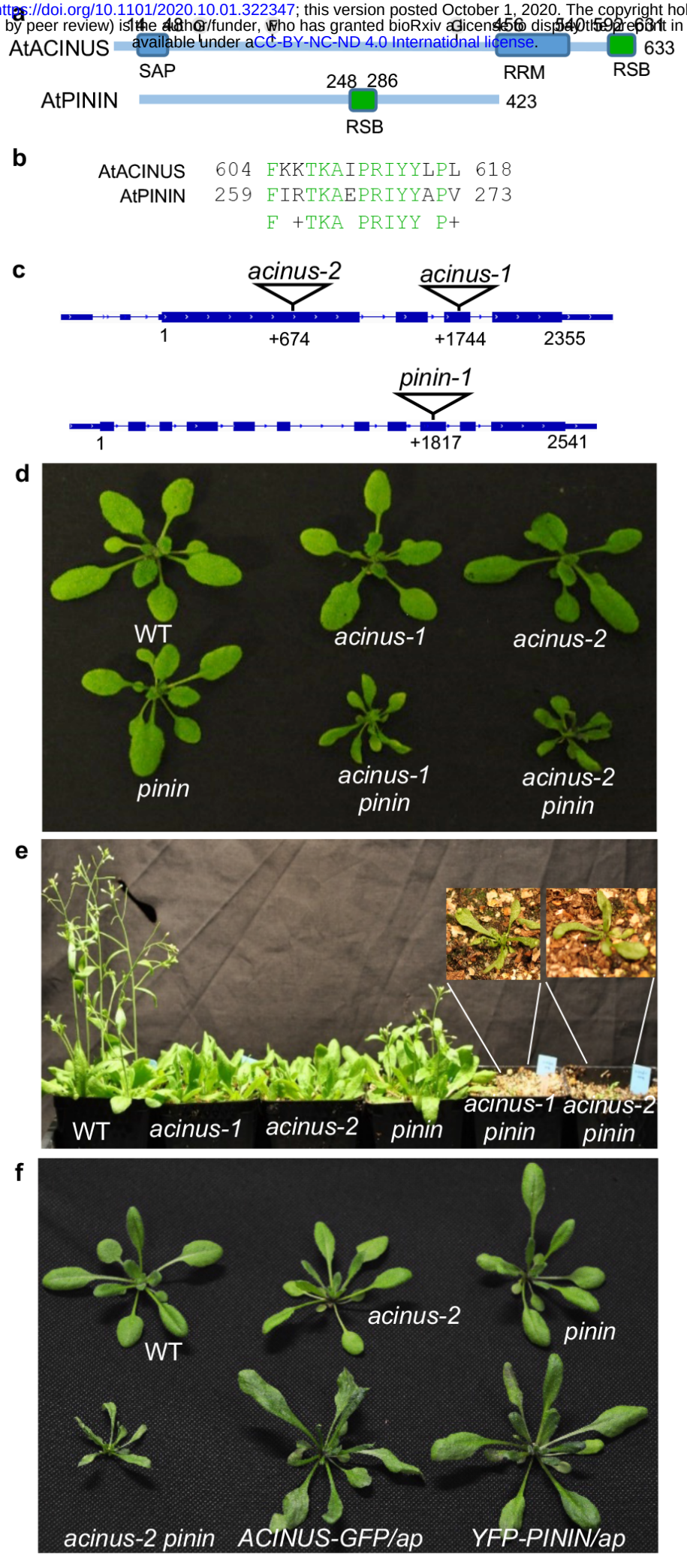

Fig.2

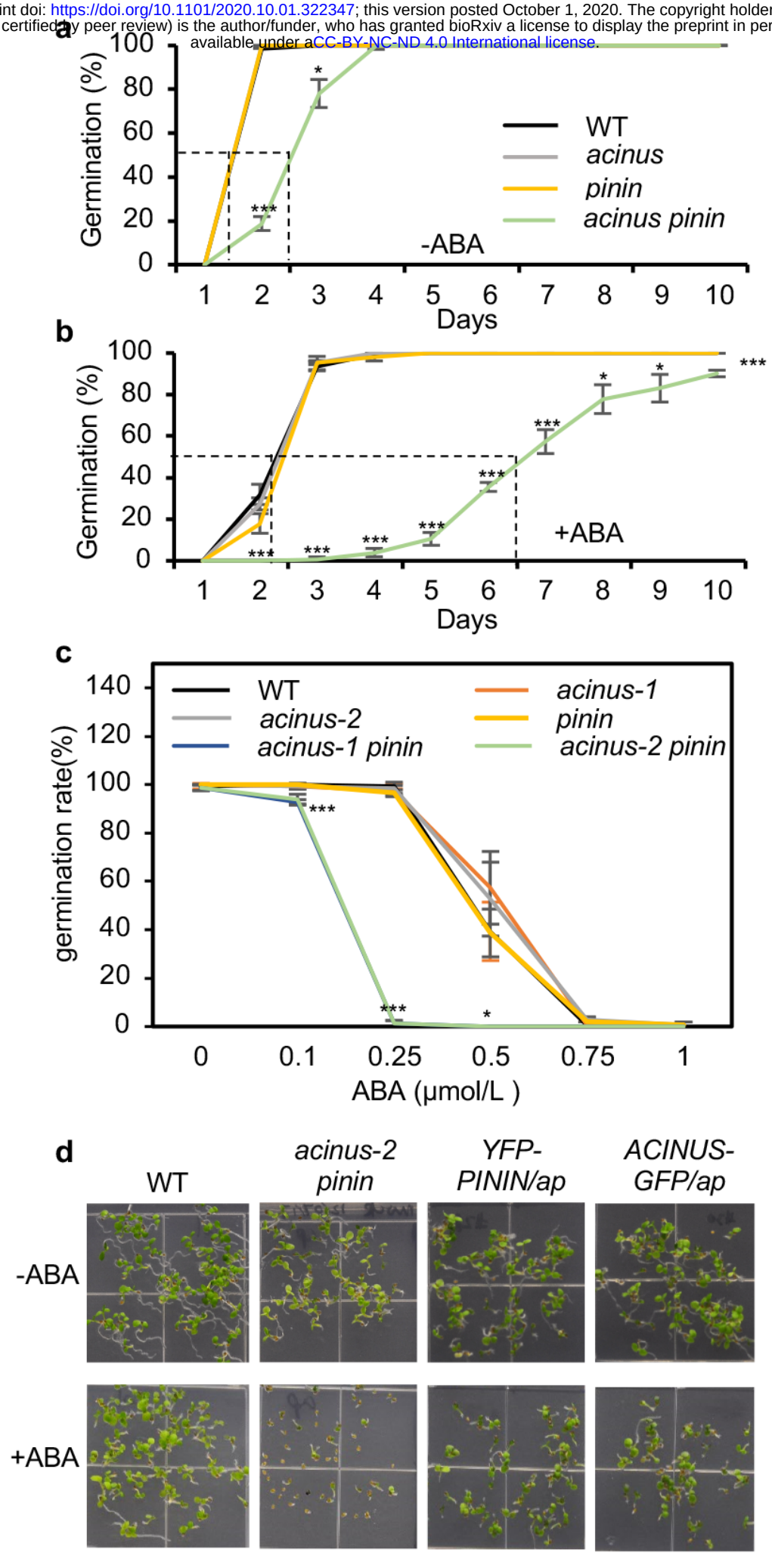

Fig.3

a

b

	Increased in *acinus pinin* (767)	Decreased in *acinus pinin*(786)
ABA-induced (1678)	144	74
ABA-repressed (1581)	43	78

Fig.4

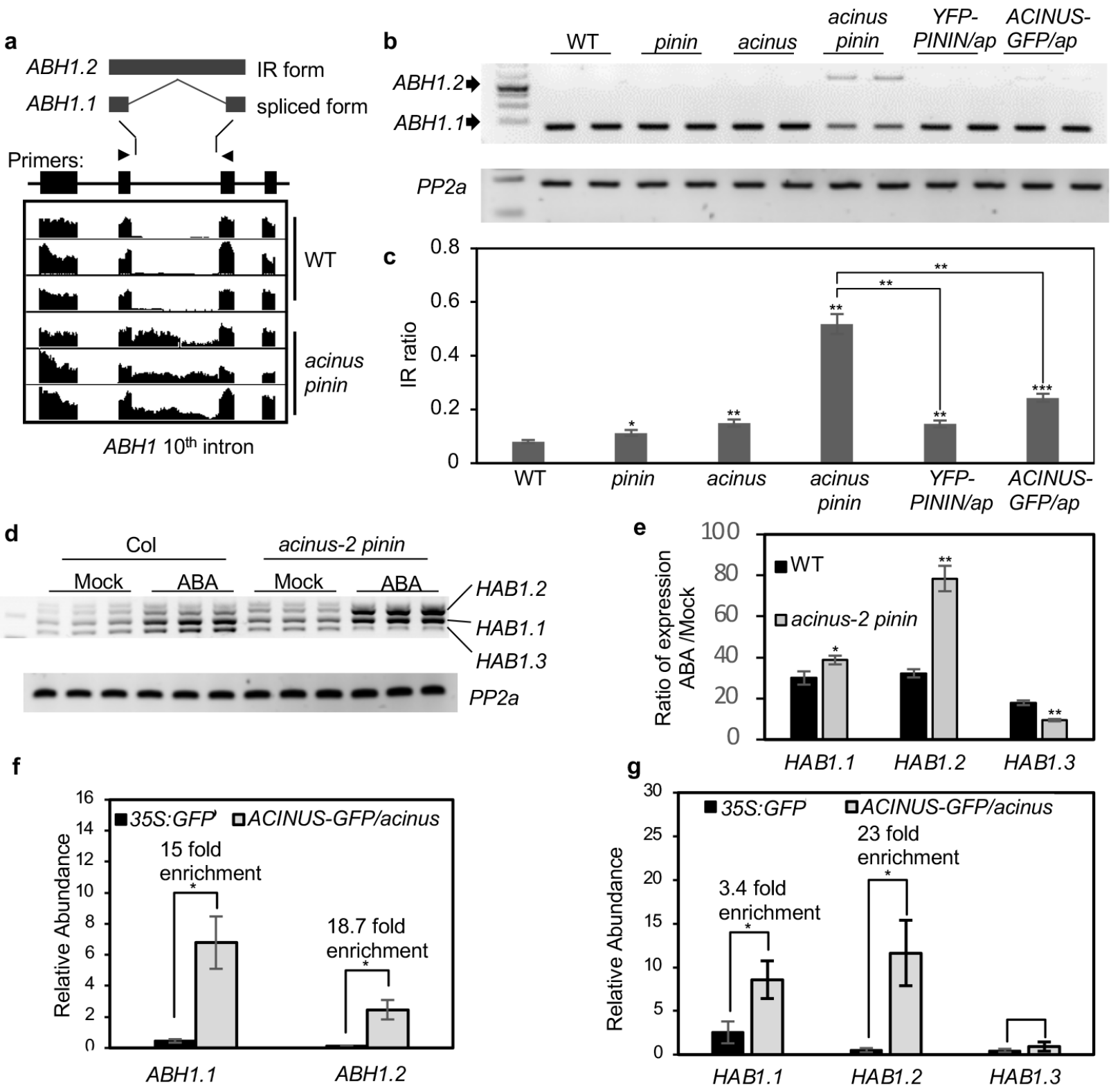

Fig.5

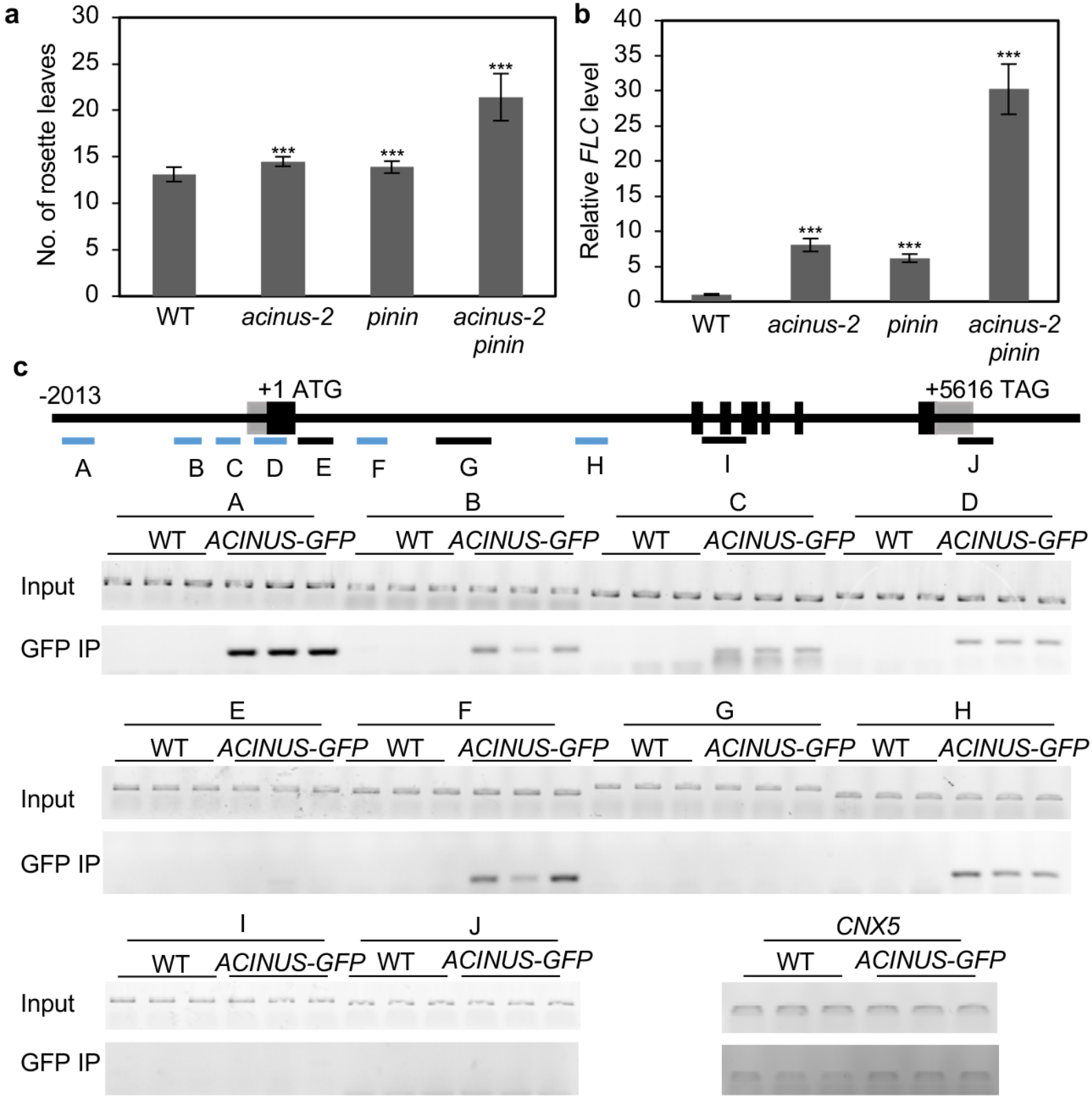

Fig.6

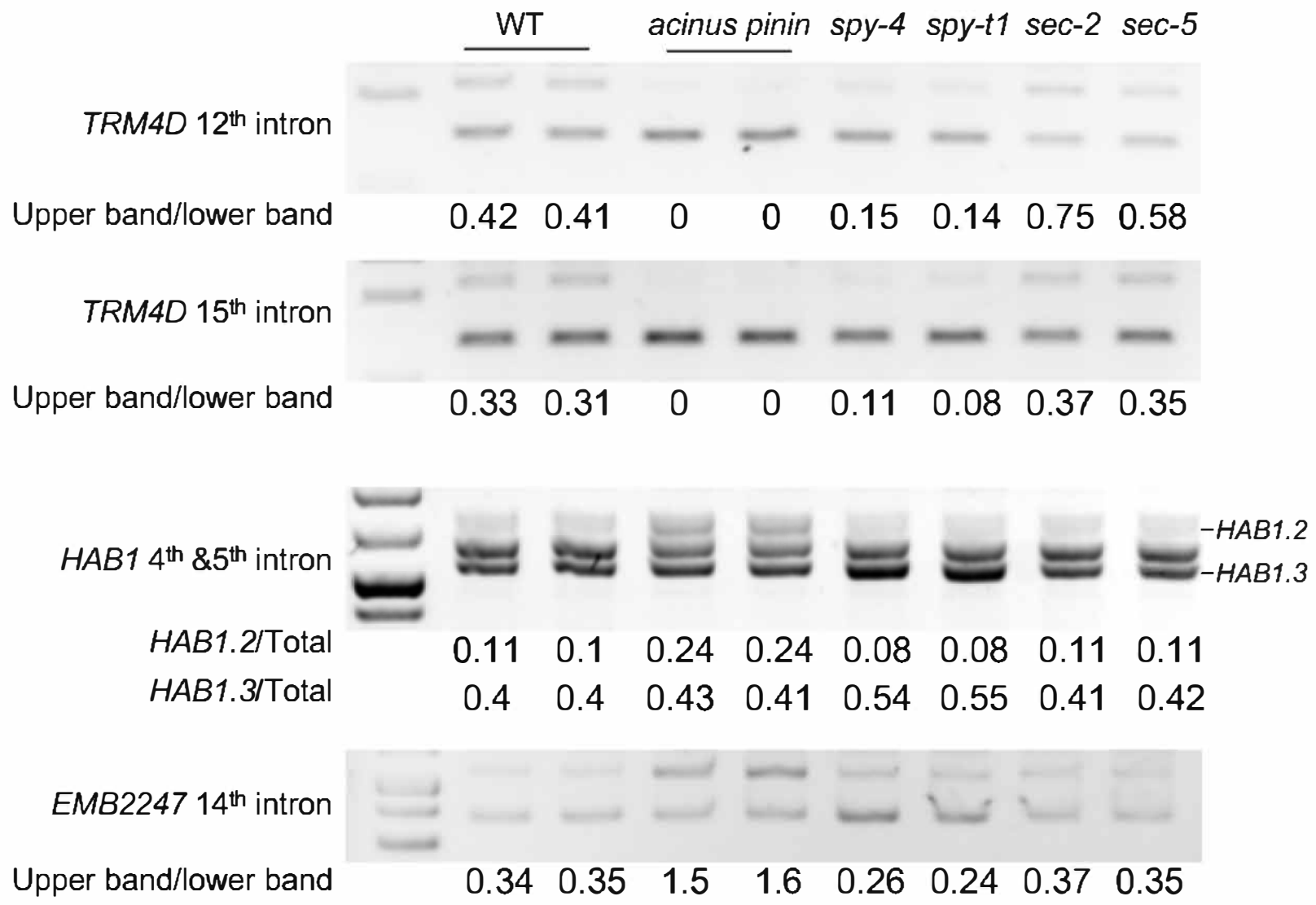

Fig.7

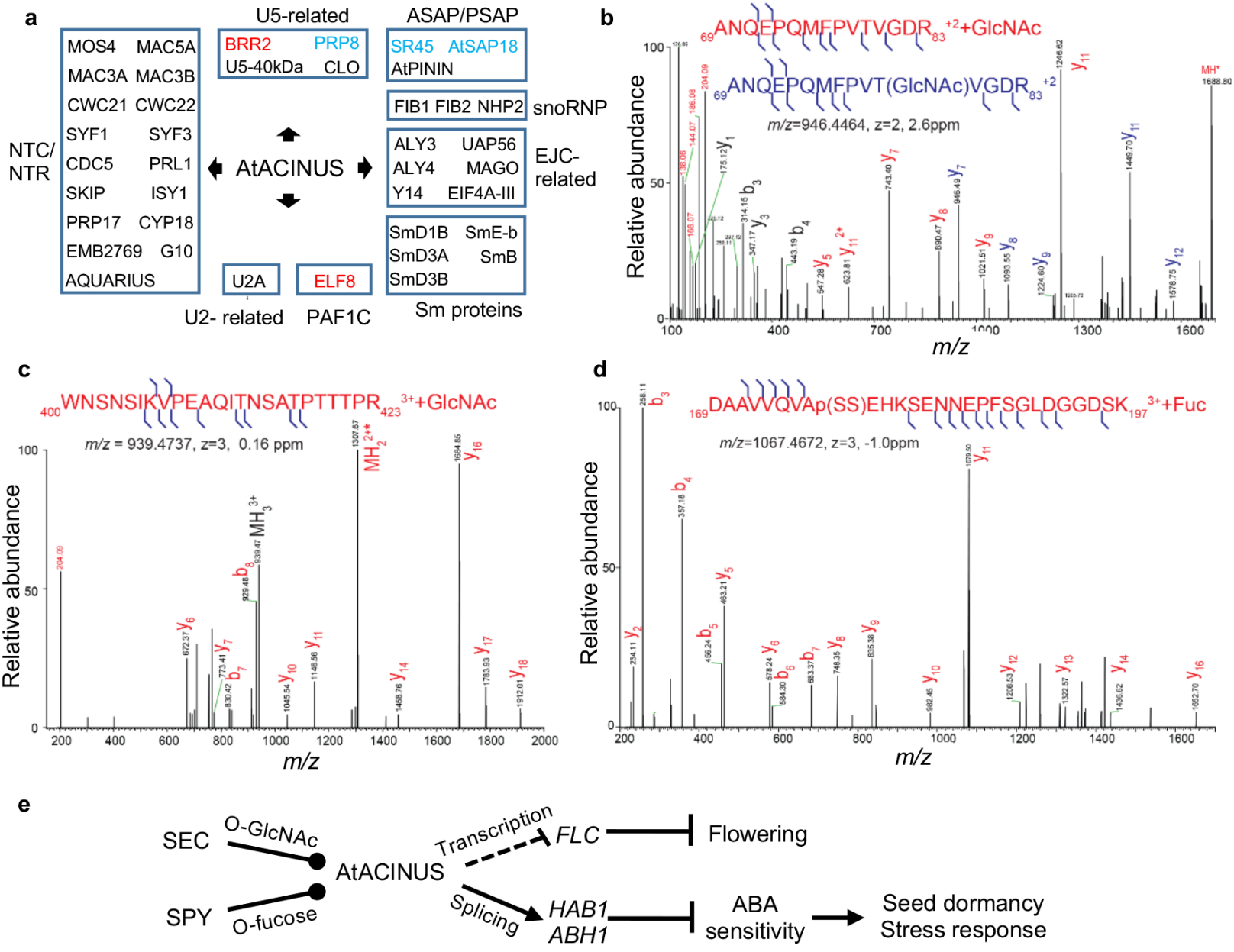

a Alignment of Acinus and AtACINUS, around SAP domain

Score	Expect	Method	Identities	Positives	Gaps
34.3 bits(77)	3e-05	Compositional matrix adjust.	18/41(44%)	25/41(60%)	0/41(0%)

```
Acinus: 66   TLDGKPLQALRVTDLKAALEQRGLAKSGQKSALVKRLKGAL  106
             LD +P+   +VT+LK  L++R L   G K  LV+RL  AL
AtACINUS:8   VLDNRPIDKWKVTELKEELKRRRLTTRGLKEELVRRLDEAL  48
```

Alignment of Acinus and AtACINUS, around RRM domain

Score	Expect	Method	Identities	Positives	Gaps
90.1 bits(222)	2e-22	Compositional matrix adjust.	35/82(43%)	58/82(70%)	2/82(2%)

```
Acinus: 1011  SNIVHISNLVRPFTLGQLKELLGRTGTLVEEAFWIDKIKSHCFVTYSTVEEAVATRTALH  1070
              +N + I   +RPFTL  ++ELLG+TG +   +FW+D IK+HC+V+Y +VEEA ATR A++
AtACINUS: 456 TNSLRIDRFLRPFTLKAVQELLGKTGNVT--SFWMDHIKTHCYVSYPSVEEAAATREAVY  513

Acinus: 1071  GVKWPQSNPKFLCADYAEQDEL  1092
               ++WP +  + L A++   +E+
AtACINUS: 514 NLQWPPNGGRHLIAEFVRAEEV  535
```

Alignment of Acinus and AtACINUS, around RSB domain

Score	Expect	Method	Identities	Positives	Gaps
44.3 bits(103)	3e-08	Compositional matrix adjust.	18/29(62%)	23/29(79%)	0/29(0%)

```
Acinus: 1211  LDDLFRKTKAAPCIYWLPLTDSQIVQKEA  1239
              LDDLF+KTKA P IY+LPL++ Q+  K A
AtACINUS: 600 LDDLFKKTKAIPRIYYLPLSEEQVAAKLA  628
```

b Alignment of Pinin and AtPININ, around RSB domain

Score	Expect	Method	Identities	Positives	Gaps
67.4 bits(163)	3e-16	Compositional matrix adjust.	45/122(37%)	69/122(56%)	10/122(8%)

```
Pinin: 132  QNMDEKGKQRNRRIFGLLMGTLQKFKQEST--VATERQKRRQEIEQKLEVQAEEERKQVE  189
            +N D K   RNRR+ G L+GTL+KF++E      T+   RR    Q+ E +A EE +++
AtPININ: 153 KNEDPKLVNRNRRMLGNLLGTLEKFRKEDKQRSGTDAYARRTAALQRAEEKAREESERLR  212

Pinin: 190  NERRELFEERRAKQTELRLL-----EQKVELAQLQEEWNEHNAKIIKYIRTKTKPHLFY  243
             + RE   E+R +   LR         ++K+EL  LQ  W+EH  K+  +IRTK +P ++Y
AtPININ: 213 LQERENLTEKRRRDLTLRARVAAKAEQKKLELLFLQ--WSEHQKKLSNFIRTKAEPRIYY  270

Pinin: 244  IP  245
             P
AtPININ: 271 AP  272
```

c

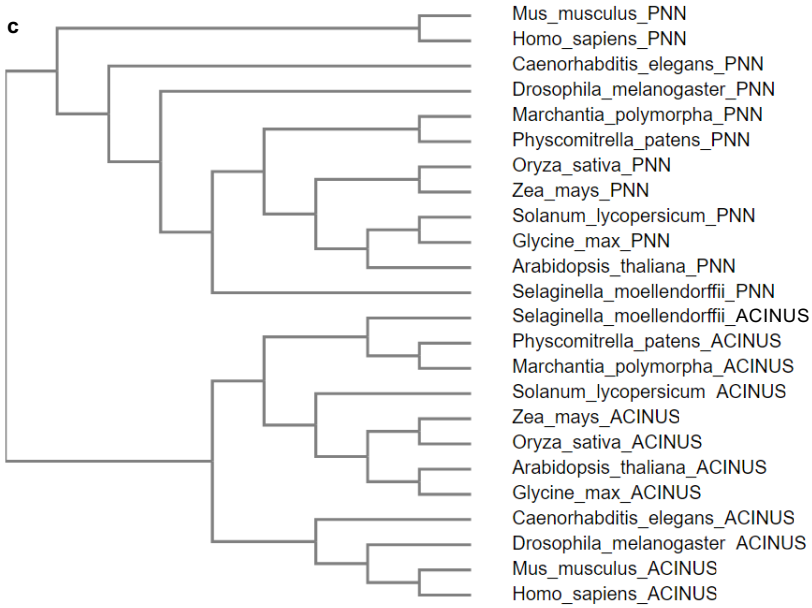

Supplementary Fig. 1 | Protein sequence analysis of AtACINUS and AtPININ. (a,b) Pairwise sequence alignment between human Acinus and AtACINUS and between human Pinin and AtPININ using Blastp from NCBI blastp suite. Hits with E value<0.01 are shown. **(c)** Dendrogram of AtACINUS and AtPININ homologs from various species. PNN=PININ.

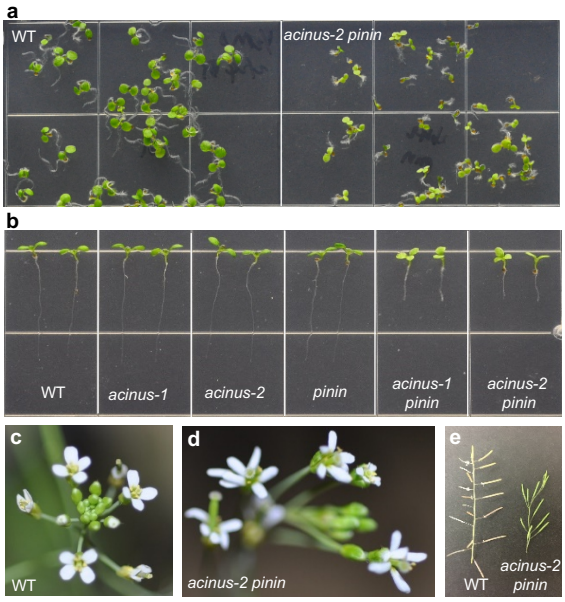

Supplementary Fig. 2 | Pleiotropic developmental defects in the *acinus-2 pinin-1* mutant. (a) Germination of *acinus-2 pinin-1* seeds was slightly delayed compared to WT. **(b)** The *acinus-2 pinin-1* mutants showed short root and tri-cotyledon phenotypes. **(c,d)** The *acinus-2 pinin-1* double mutant (d) showed increased number of petals compared to WT (c). **(e)** The *acinus-2 pinin-1* double mutant (right) showed phyllotaxis defects compared to WT (left).

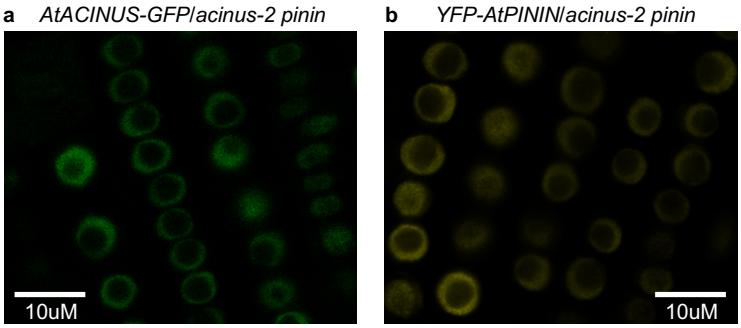

Supplementary Fig. 3 | Confocal image of AtACINUS-GFP localization in the root of *AtACINUS-GFP*/*acinus-2 pinin-1* seedlings (a) and YFP-PININ localization in the root of *YFP-PININ*/*acinus-2 pinin-1* seedlings (b).

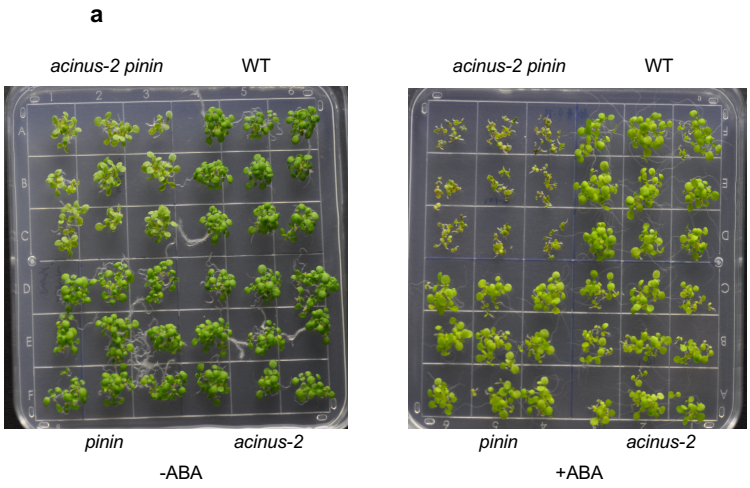

Supplementary Fig. 4 | AtACINUS and AtPININ redundantly inhibit ABA responses. (a) Post-germination seedling growth is inhibited by ABA in *acinus-2 pinin-1*. Seeds of WT, *acinus-2*, *pinin-1* and *acinus-2 pinin-1* were germinated on filtered paper, transferred to medium containing no ABA or 1µmol/L ABA for 5 days. **(b)** Germination rate of the indicated genotypes after six days on ½ MS medium containing 0 or 0.5 µmol/L ABA. Error bars indicate SD calculated from 3 biological replicates (n=3). The data points of wild-type, *acinus-2* and *pinin-1* overlap. Asterisks indicate significant differences to wild type (two-sided Student's t-test, *P< 0.05, ** P< 0.01, *** P< 0.001).

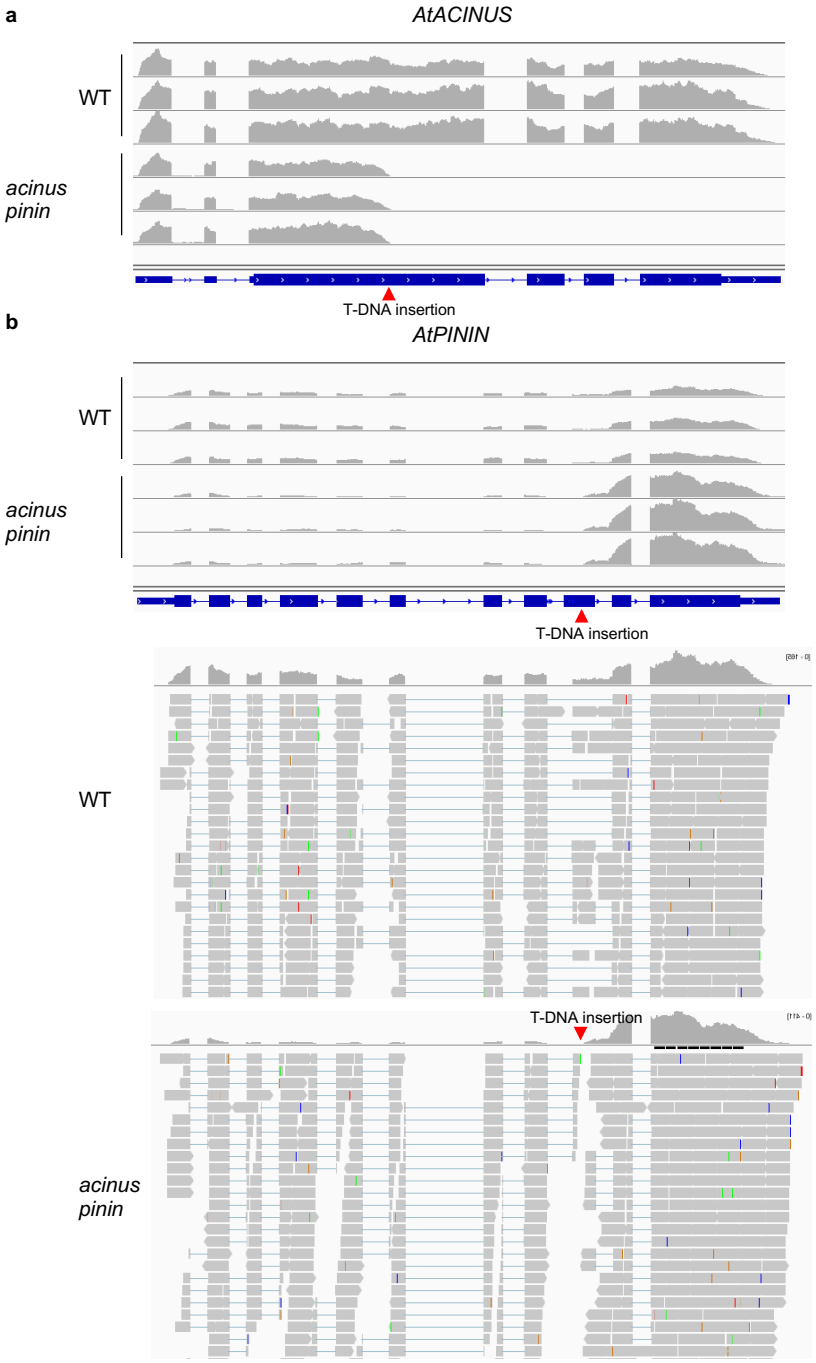

Supplementary Fig. 5 | Full length *AtACINUS* and *AtPININ* were not transcribed in *acinus-2 pinin-1*. (a) A partial *AtACINUS* transcript from the 5' transcription start site until T-DNA insertion site was detected in *acinus-2 pinin-1*. **(b)** A partial *AtPININ* transcript from the 5' transcription start site until T-DNA insertion site was detected at a reduced level in *acinus-2 pinin-1*. Transcription was initiated from the T-DNA insertion to transcribe the 3' end of *AtPININ* after the T-DNA insertion site at an increased level. However, there was no full length *AtPININ* produced because transcripts were discontinuous and showed a gap in the 9th exon at the position marked by the red triangle. No reads spanning (gray bar or blue line) this region was detected in *acinus-2 pinin-1* while a large number of reads spanning this region were detected in wild-type.

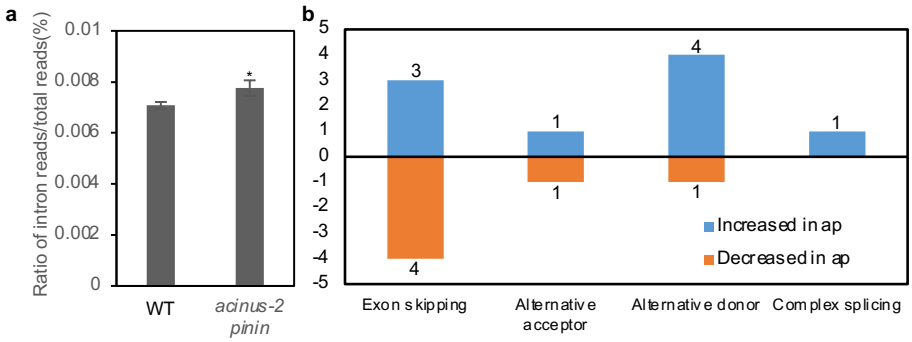

Supplementary Fig. 6 (**a**) The percentage of intron reads in WT and the *acinus-2 pinin-1* double mutant. Error bars indicate SD calculated from 3 biological replicates (n=3). (**b**) A summary of other types of splicing defects in *acinus-2 pinin-1* compared to WT. Asterisks indicate significant differences to wild type (two-sided Student's t-test, *P< 0.05, ** P< 0.01, *** P< 0.001).

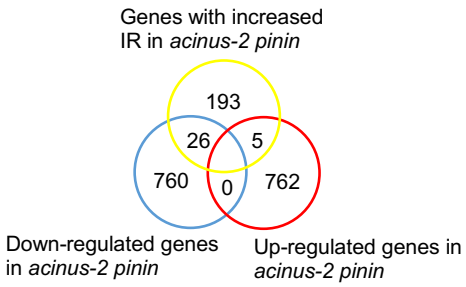

Supplementary Fig. 7 | Overlap between differentially expressed genes in *acinus-2 pinin-1* and genes with increased intron retention in *acinus-2 pinin-1*.

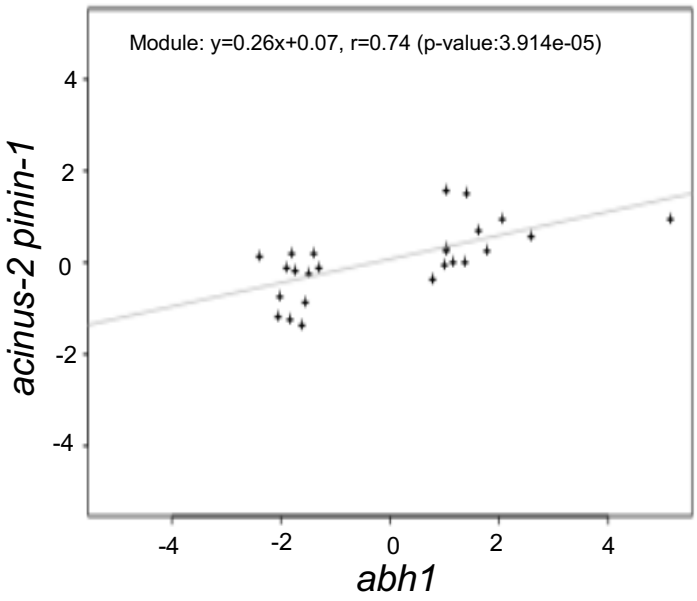

Supplementary Fig. 8 | The genes mis-expressed in *abh1* (data from Kuhn *et al*., 2008 [32]) show a strong correlation to genes mis-regulated in *acinus-2 pinin-1*, with Spearman's correlation=0.74.

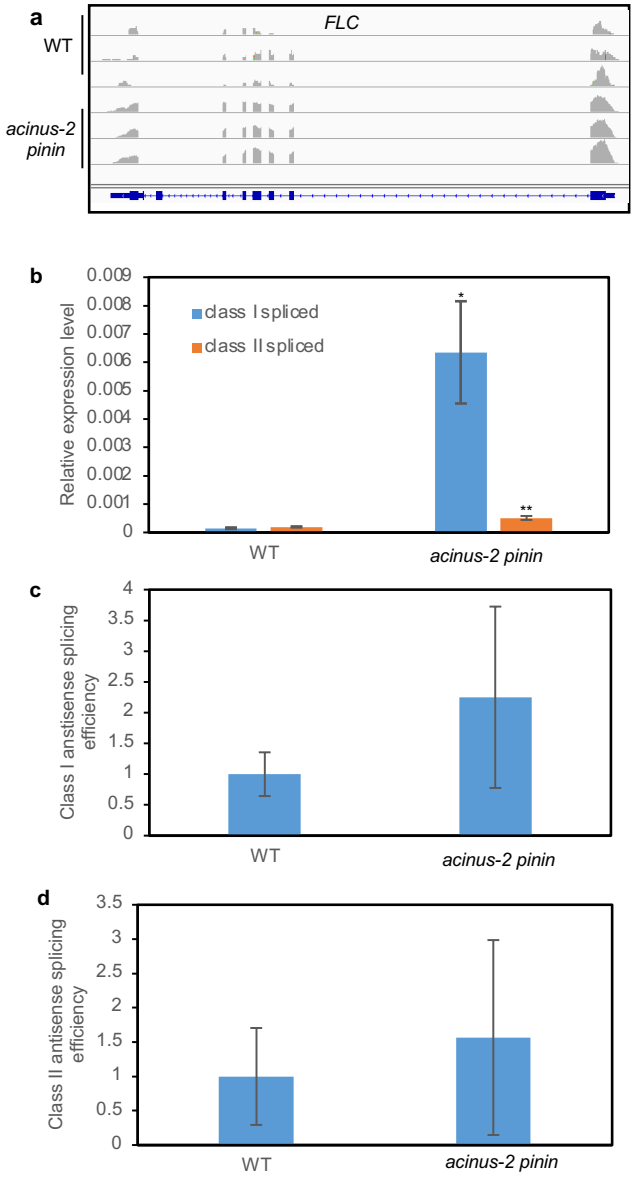

Supplementary Fig. 9 | *FLC* antisense I is increased relative to antisense II in *acinus-2 pinin-1* while the splicing efficiency is not significantly changed. (a) Reads coverage of *FLC* locus in WT and *acinus-2 pinin-1*. Track height is set to 15 in WT and 200 in *acinus-2 pinin-1*. **(b)** Expression levels of *FLC* spliced class I antisense and spliced class II antisense relative to *PP2A* in wild-type and *acinus-2 pinin-1*. **(c)** Class I antisense splicing efficiency calculated from class I spliced/class I unspliced. WT is set to 1. **(d)** Class II antisense splicing efficiency calculated from class II spliced/class II unspliced. WT is set to 1. In our experimental conditions, only class II-II is detected and used for calculation for class II antisense. RNA was extracted from 12-day-old seedlings. Error bars indicate SD calculated from 3 biological replicates (n=3). Asterisks indicate significant differences to wild type (two-sided Student's t-test, *P< 0.05, ** P< 0.01, *** P< 0.001).

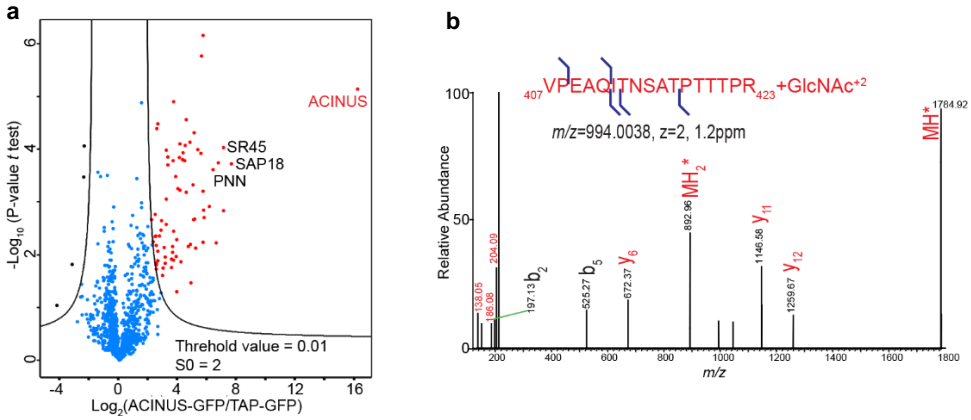

Supplementary Fig. 10 | (a) Volcano plot of the IP-MS analysis of the AtACINUS interactome. The logarithmic ratios of protein signal intensities between AtACINUS-GFP and TAP-GFP (negative control) are plotted against negative logarithmic p-values of the *t*-test of triplicate IP-MS. The hyperbolic curves are based on an FDR estimation 0.01 and S0=2. The curves separate bait AtACINUS and its specific interactors (red dots) from background proteins (blue dots) and possible false positive (black dots) that are enriched in the TAP-GFP control. Additional information is in Supplemental Data 1. **(b)** HCD spectra detected O-GlcNAcylation on a sequence spanning amino acid 407 to 423 of AtACINUS with neutral loss.

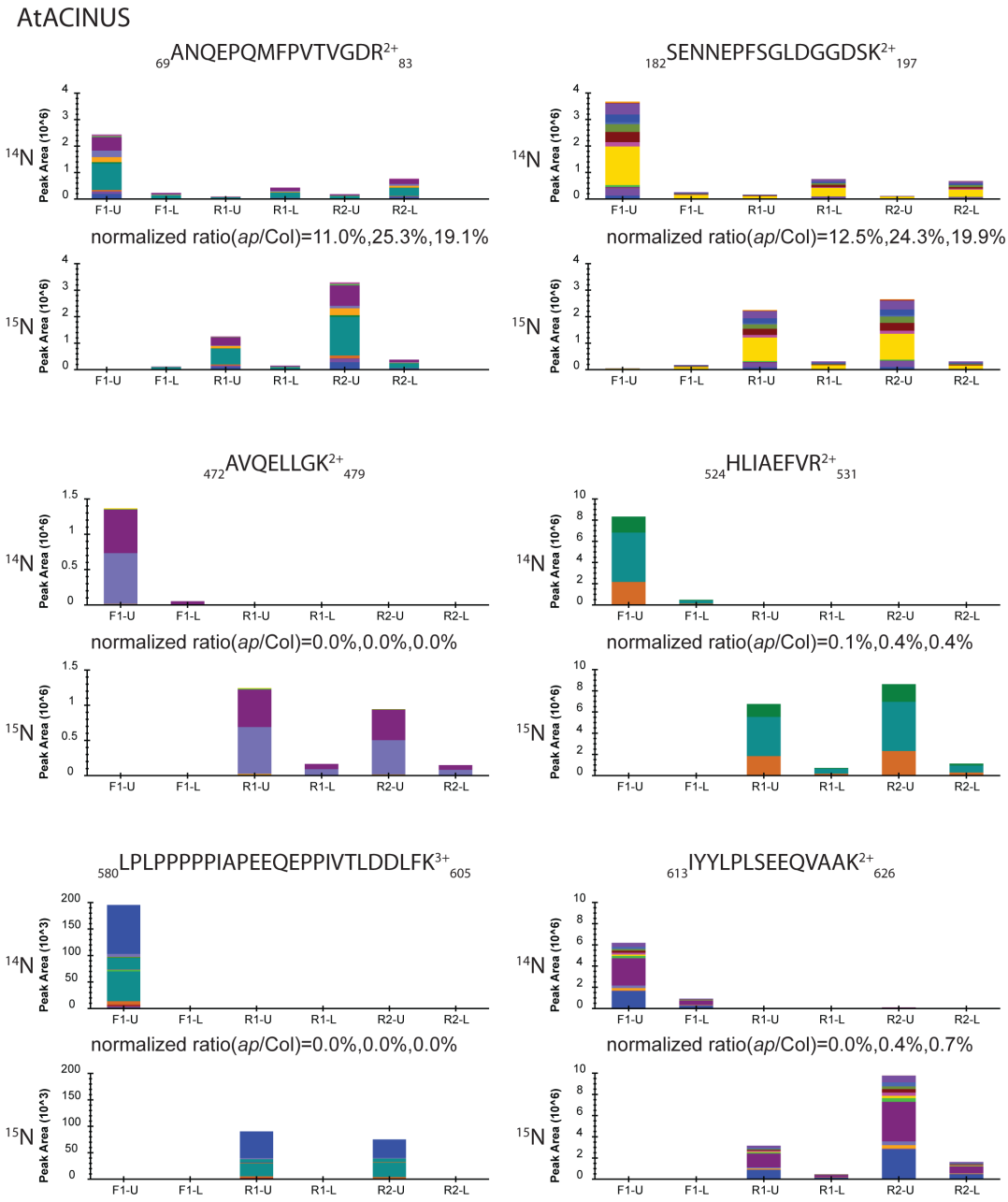

Supplementary Fig.11| Targeted quantifications using Parallel Reaction Monitoring (PRM) show AtACINUS N-terminal has reduced expression and C-terminal is undetectable in *acinus-2 pinin-1* mutant. Two gel segments (upper part (U) and lower part(L)) were excised from each mixed samples and subjected to trypsin digestion. Proteins were quantified from both segments of each mixed sample, including F1 (^{14}N Col/ ^{15}N *acinus-2 pinin-1*) and R1, R2 samples (^{14}N *acinus-2 pinin-1*/ ^{15}N Col). Peak areas of fragments were extracted for the ^{14}N and ^{15}N labeled peptides of targeted proteins using 5 ppm mass window and integrated across the elute profile using Skyline platform. The sum of peak areas from two segments were calculated from Col and *acinus-2 pinin-1* peptides and ratios were calculated and normalized to TUBULIN2.

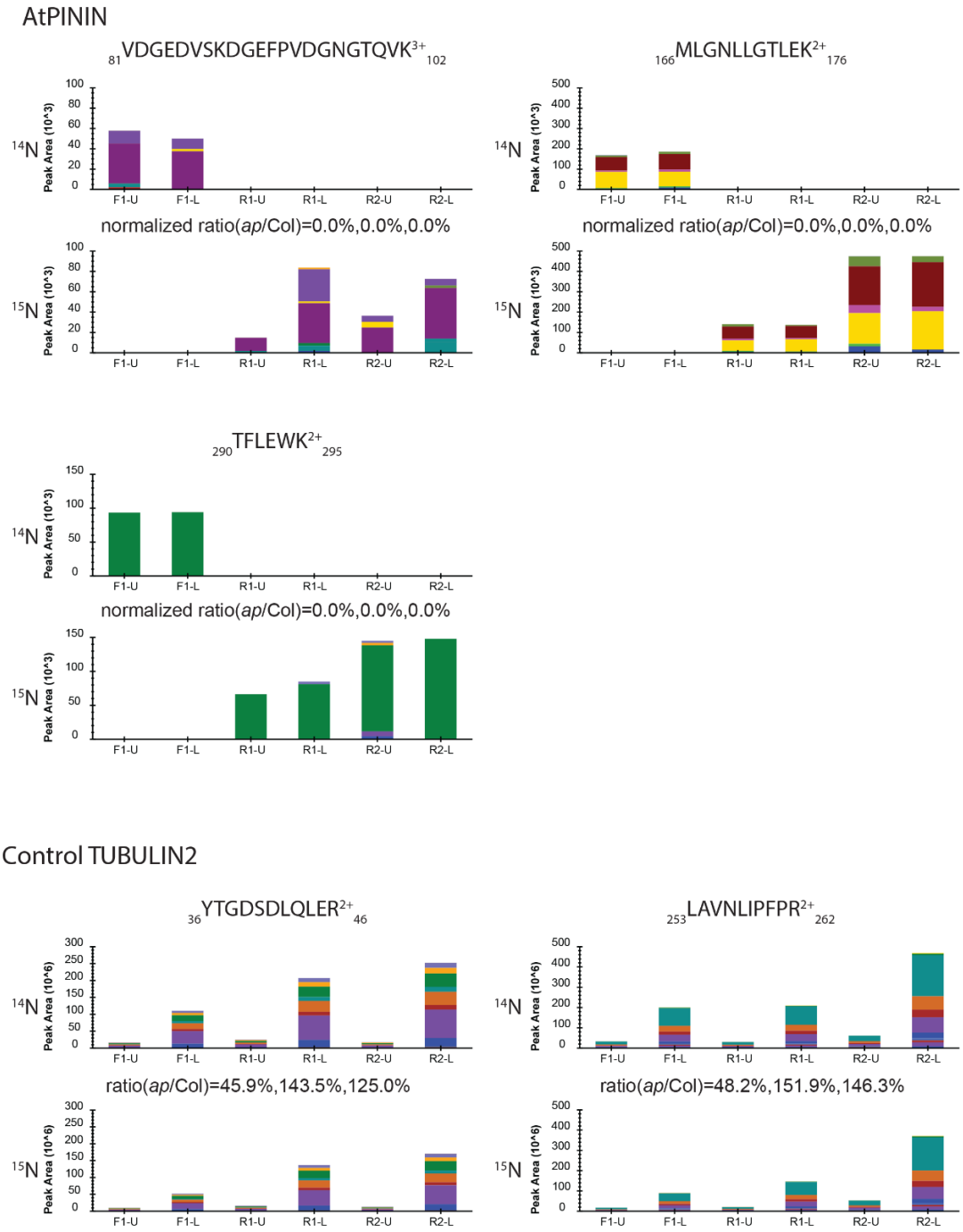

Supplementary Fig.12| Targeted quantifications using Parallel Reaction Monitoring (PRM) show AtPININ protein level is non-detectable in *acinus-2 pinin-1* mutant. Two gel segments (upper part (U) and lower part(L)) were excised from each mixed samples and subjected to trypsin digestion. Proteins were quantified from both segments of each mixed sample, including F1 (^{14}N Col/ ^{15}N *acinus-2 pinin-1*) and R1, R2 samples (^{14}N *acinus-2 pinin-1*/ ^{15}N Col). Peak areas of fragments were extracted for the ^{14}N and ^{15}N labeled peptides of targeted proteins using 5 ppm mass window and integrated across the elute profile using Skyline platform. The sum of peak areas from two segments were calculated from Col and *acinus-2 pinin-1* peptides and ratios were calculated and normalized to TUBULIN2.

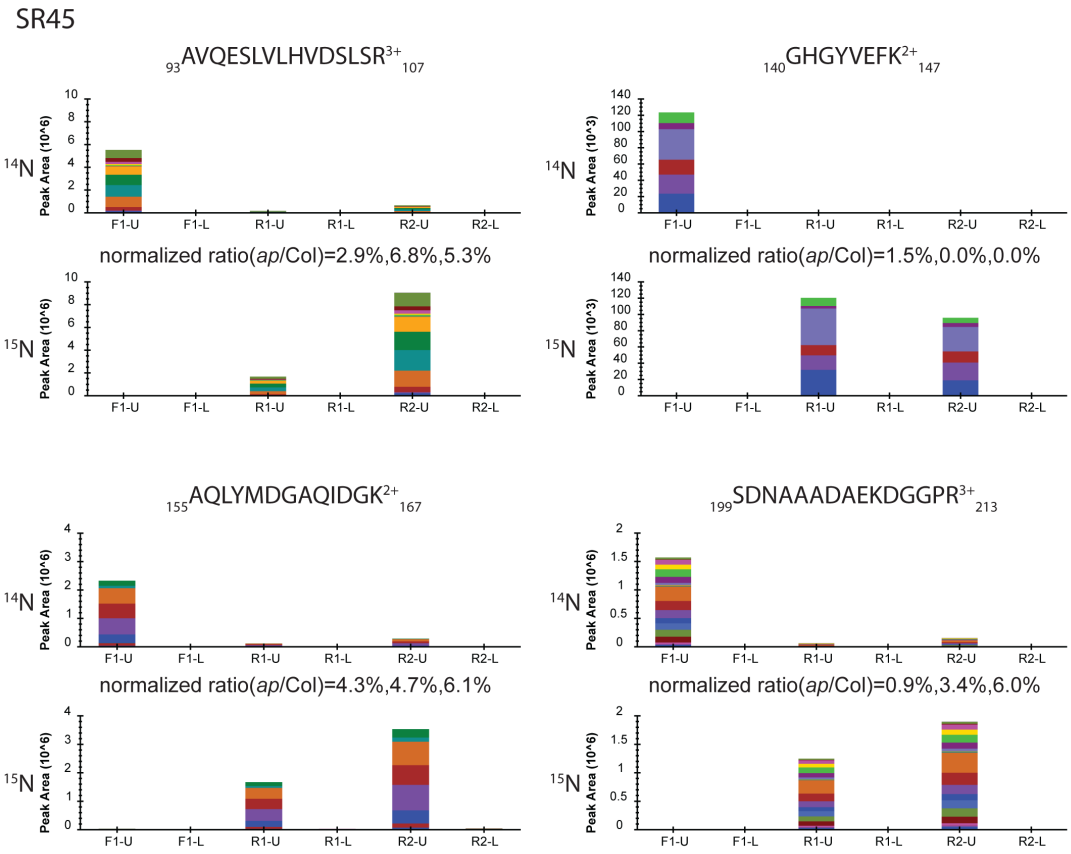

Supplementary Fig.13| Targeted quantifications using Parallel Reaction Monitoring (PRM) show much reduced SR45 protein levels in *acinus-2 pinin-1* mutant. Two gel segments (upper part (U) and lower part(L)) were excised from each mixed samples and subjected to trypsin digestion. Proteins were quantified from both segments of each mixed sample, including F1 (^{14}N Col/ ^{15}N *acinus-2 pinin-1*) and R1, R2 samples (^{14}N *acinus-2 pinin-1*/ ^{15}N Col). Peak areas of fragments were extracted for the ^{14}N and ^{15}N labeled peptides of targeted proteins using 5 ppm mass window and integrated across the elute profile using Skyline platform. The sum of peak areas from two segments were calculated from Col and *acinus-2 pinin-1* peptides and ratios were calculated and normalized to TUBULIN2.

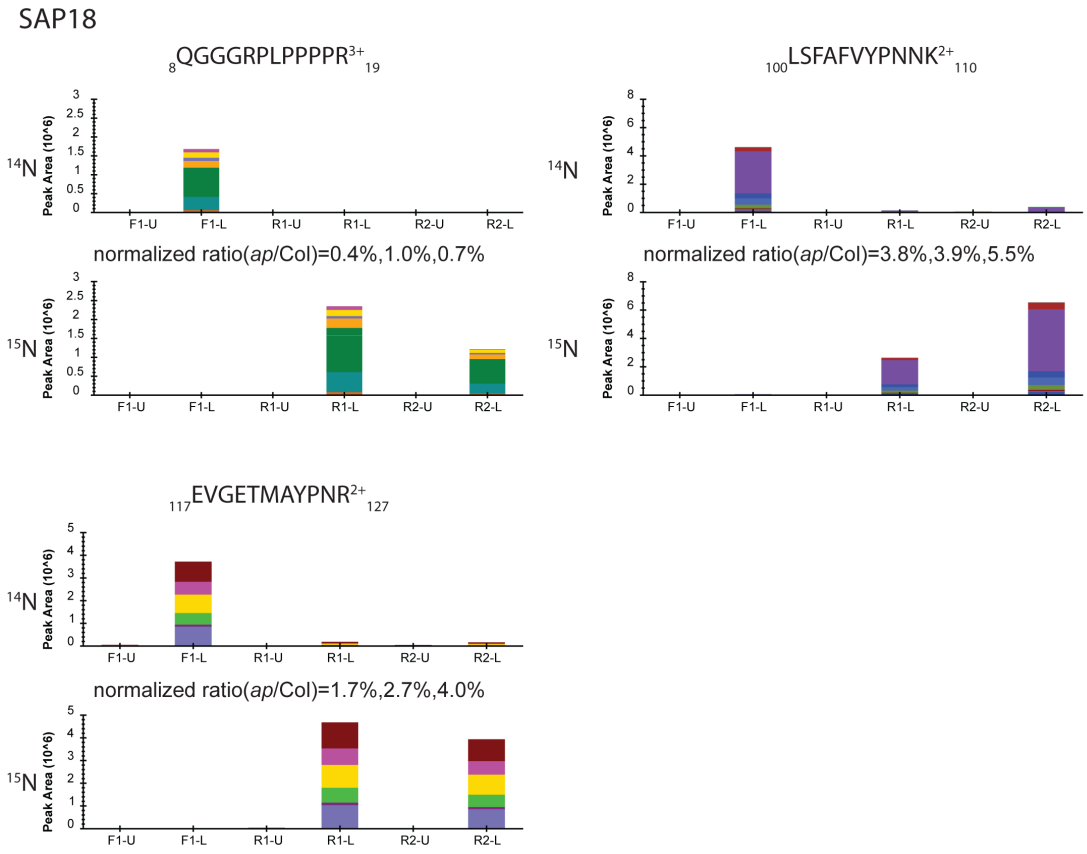

Supplementary Fig.14| Targeted quantifications using Parallel Reaction Monitoring (PRM) show much reduced SAP18 protein levels in *acinus-2 pinin-1* mutant. Two gel segments (upper part (U) and lower part(L)) were excised from each mixed samples and subjected to trypsin digestion. Proteins were quantified from both segments of each mixed sample, including F1 (^{14}N Col/ ^{15}N *acinus-2 pinin-1*) and R1, R2 samples (^{14}N *acinus-2 pinin-1*/ ^{15}N Col). Peak areas of fragments were extracted for the ^{14}N and ^{15}N labeled peptides of targeted proteins using 5 ppm mass window and integrated across the elute profile using Skyline platform. The sum of peak areas from two segments were calculated from Col and *acinus-2 pinin-1* peptides and ratios were calculated and normalized to TUBULIN2.

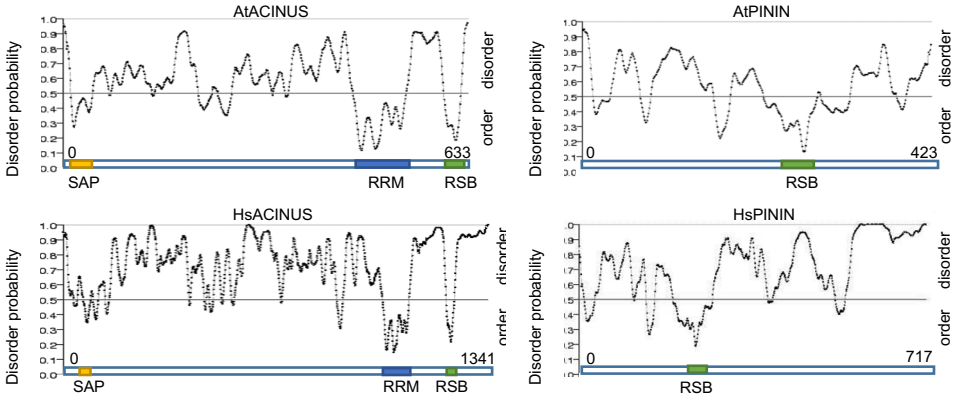

Supplementary Fig. 15 | ACINUS and PININ are predicted to be highly disordered proteins with small ordered regions that overlap with functional domains.

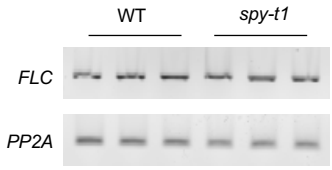

Supplementary Fig.16 Semi-quantitative RT-PCR of *FLC* in WT and *spy-t1*. *PP2A* serves as an internal control.